A two-layer model for stratocumulus clouds

September 10, 2014

Author:
L.E.M. Vlot

Supervisor:
Dr. S.R. de Roode

Cover picture by Ryan [2012].

Members of the thesis committee
Prof. dr. A. Pier Siebesma
Dr. Stephan R. de Roode
Dr. Yann Dufournet
Ir. Johan J. van der Dussen

Abstract

Mixed layer models (MLMs) have been used to improve the understanding of stratocumulus clouds. These models consider the stratocumulus-topped boundary layer as a single well-mixed slab and only require the surface and top fluxes and a source/sink term to describe the boundary layer. Stratocumulus dynamics and the influence of large-scale conditions such as the sea surface temperature on the stratocumulus cloud amount have been studied with MLMs.
Observations show that the boundary layer does not remain well-mixed when it deepens. Instead of a single mixed layer, it can be considered as two mixed layers on top of each other. This observed two-layer structure motivates to build a new model including a seperate cloud and sub-cloud layer: the two-layer model.
The two-layer model is used to study the stratocumulus to cumulus transition and is found to be capable of predicting this transition. The effect of subsidence on the liquid water path (LWP) was examined. A higher subsidence leads to a smaller LWP and a more rapid break-up of the stratocumulus clouds.
Steady-state solutions of the two-layer model showed that the change of LWP due to a warmer climate is smaller than predicted with a MLM. Where the MLM only predicts a cloud thickening, the two-layer model predicts thinning as well as thickening depending on the free tropospheric conditions.

This thesis has been conducted as a final work for the master Applied Physics at the section of Atmospheric Physics of the TU Delft.

Contents

1 Introduction

Stratocumulus clouds are a shallow, low-level cloud type, typically occurring below two kilometers and with a thickness in the order of a few hundred meters. An example of a stratocumulus cloud can be seen in figure 1.1. Stratocumulus clouds are part of the atmospheric boundary layer, which is the shallow layer close to the earth where the earth surface is 'felt'. The atmospheric boundary layer is a layer of turbulent air that is separated from the lighter, laminar air above.
Shallow stratocumulus-topped boundary layers (STBLs) are often well mixed, but for deeper boundary layers the STBL begins to separate into two layers where cumulus clouds start to form underneath the stratocumulus clouds [Bretherton and Wyant, 1997].

Figure 1.1 – A sheet of stratocumulus clouds. Image from Met Office UK [2014].

Stratocumuli cover approximately one fifth of the Earth's surface in the annual mean [Wood, 2012], whereas the 80 % of the stratocumulus are located over the ocean [Warren et al., 1988]. Stratocumuli have a strong ability to cool our planet by reflecting solar radiation due to their high albedo compared to the underlying sea surface and large coverage [Dal Gesso et al., 2014b].

In climate predictions, the most uncertainties arise from the stratocumulus and stratocumulus to cumulus transition regimes [Williams and Webb, 2009]. According to Randall et al. [1984] small changes in the coverage and thickness of stratocumulus clouds lead to an offset in climate warming due to enhanced greenhouse gasses.

While stratocumulus clouds now exert a cooling effect on the planet, this cooling effect may be enhanced or weakened in response to global warming, thereby producing a radiative feedback. It is therefore important to see how the stratocumulus amount changes due to climate warming.

Earlier research regarding the cloud-climate feedback has been done in several ways. The physical processes concerning low-level clouds have been studied by an intercomparison study between LES and single column models (SCMs) by Zhang et al. [2013]. They examined the steady-state response of perturbations in cloud controlling factors for three cloud regimes: well-mixed stratocumulus, decoupled stratocumulus, and cumulus.
The different LES models produce results that are consistent with each other and predict a positive cloud radiative feedback in a warmed climate for both stratocumulus and cumulus underneath stratocumulus cases, but there is a large spread in the outcomes of the SCMs both in sign and magnitude.

De Roode et al. [2012] studied the steady-state liquid water path (LWP) response of the stratocumulus-topped boundary layer to an increase in SST, using the MLM. They found that the entrainment response due to an increase in SST can be positive or negative, depending on the free tropospheric conditions. The response of the LWP can be magnified, damped or change in sign due to this entrainment response. The different parameterisations of entrainment in climate models may therefore be a plausible cause of the spread in LWP-response prediction.

Although the MLM is a suitable tool to examine well-mixed layers, it is less suitable for more complex situations such as a deepened boundary layer where stratocumulus and cumulus clouds co-exist. Observations of these cases show that the atmosphere is closer to a two-layer structure, with a warmer and dryer cloud layer as compared to the cooler and more humid sub-cloud layer below. In this research a new model is developed to describe this two-layered structure. This two-layer model is built out of two different mixed layers on top of each other.
The two-layer model can be used to gain more understanding of the STBL and to study the effect of changes in large-scale conditions on the STBL.

To validate the two-layer model LES results from a stratocumulus to cumulus transition experiment are used, the Atlantic Stratocumulus Transition EXperiment (ASTEX). Because of the uncertainty in the subsidence rate during the transition [Bretherton and Pincus, 1995], a subsidence sensitivity experiment will be performed with the two-layer model. Where Bretherton and Pincus argued that decreasing the subsidence led to a more rapid break-up of the cloud layer, more recent subsidence sensitivity experiments found the opposite [Sandu and Stevens, 2011, Bretherton et al., 2013].

Besides these transient experiments, steady-state experiments are performed in addition to the experiments of de Roode et al.. The response of the LWP to a warming climate is examined, but now with a two-layer model instead of an MLM.

2 Thermodynamics

The presence of variable amounts of water in the atmosphere has two important effects. Firstly, it modifies the density which is the major forcing term for vertical momentum. Secondly, formation and dissipation of clouds lead to latent heat release effects, that are relevant to the heat budget of the atmosphere. In this chapter, thermodynamic laws will be used to incorporate the effects of moisture on heat and density and to obtain variables that are conserved under adiabatic processes. To indicate the amount of water dimensionless measures as the mixing ratio r or the specific humidity q can be used. The mixing ratio is a ratio of the mass of water to the mass of dry air, whereas the specific humidity is a ratio of the mass of water to the total mass of water and dry air;

$$\begin{aligned} r_k &= \tfrac{m_k}{m_d}, \\ q_k &= \tfrac{m_k}{m} \qquad \text{where } k \in v, l, i \end{aligned} \tag{2.1}$$

and with v, l and i represent the water vapor, liquid water and water in the ice phase respectively. Here m_d is the mass of dry air and the total mass of air is $m = m_v + m_l + m_i + m_d$. The total specific humidity is then defined by

$$q_t = q_v + q_l + q_i. \tag{2.2}$$

2.1 Potential temperature

Air parcels at different heights will experience different pressures p and temperatures T. To compare air parcels adequately, the potential temperature is introduced. The potential temperature θ is not influenced by vertical adiabatic movement of a dry air parcel. It is defined by

$$\theta = T \left(\frac{p_0}{p}\right)^{\frac{R_\mathrm{d}}{c_p}}, \tag{2.3}$$

where R_d is the ideal gas constant for dry air, c_p the specific heat capacity at constant pressure and p_0 the pressure at a reference height, which is usually taken $p_0 = 1000$ hPa. The derivation of equation (2.3) can be found in appendix (B.1). A more convenient way of writing is

$$\theta = \frac{T}{\Pi}, \tag{2.4}$$

with the exner function $\Pi = \left(\frac{p_0}{p}\right)^{\frac{-R_\mathrm{d}}{c_p}}$.

2.2 Liquid water potential temperature

For vertical adiabatic movement of a moist air parcel, additional effects of heating occur. If the parcel rises, at some point the specific humidity of the parcel will equal the saturation humidity. Further rising of the parcel will lead to condensation and thus in a release of latent heat. The liquid water potential temperature takes these phase changes into account and is therefore a conserved quantity for isentropic processes in cloudy atmospheres. The liquid water potential temperature is given by:

$$\theta_l = \theta - \left(\frac{L_v}{\Pi c_p}\right) q_l, \tag{2.5}$$

with L_v the specific latent heat for vaporization and q_l the liquid specific humidity [Deardorff, 1975]. The liquid temperature T_l is then again obtained from θ_l by the exner function.

2.3 Virtual potential temperature

Buoyancy is one of the driving forces for turbulence in the boundary layer. Parcels of warm air rise because they are less dense than the surrounding air, and thus positively buoyant. Virtual temperature is the temperature that dry air must have to equal the density of moist air at the same pressure and is therefore a useful variable in studies involving buoyancy. Instead of studying variations in density, variations in virtual potential temperature can be used. The virtual temperature is given by:

$$T_v = \left[1 - \left(1 - \frac{1}{\epsilon}\right) q_v - q_l\right] T, \tag{2.6}$$

with $\epsilon = \frac{R_\mathrm{d}}{R_v}$, [Stull, 1988]. The virtual potential temperature is defined as

$$\theta_v = \frac{T_v}{\Pi}. \tag{2.7}$$

2.4 Saturation humidity

The saturation vapor pressure at liquid temperature T_l is determined by the Tetens formula:

$$\begin{aligned} e_s(T_l) =& e_{s0} \exp\left[a\frac{(T_l - T_{trip})}{T_l - b}\right], \\ &\text{with} \\ e_{s0} =& 610.78 \text{ Pa}, \\ T_{trip} =& 273.16 \text{ K}, \\ a =& 17.27, \\ b =& 35.86, \end{aligned} \tag{2.8}$$

[Murray, 1967]. With the saturation vapor pressure, the saturation specific humidity at temperature T_l can be calculated:

$$q_{sat} \equiv q_s(T_l, p) = \frac{R_\mathrm{d}}{R_\mathrm{v}} \frac{e_s(T_l)}{p - 0.378 e_s(T_l)}, \tag{2.9}$$

where R_v denotes the ideal gas constant of vapor, [Cuijpers, 1994]. To obtain the saturation humidity profile in the boundary layer, the pressure profile is needed. Using the hydrostatic pressure

$$\frac{dp}{dz} = -\rho g \tag{2.10}$$

and the gas law

$$p = \rho R_\mathrm{d} T_v \longrightarrow \rho = \frac{p}{R_\mathrm{d} T_v} \tag{2.11}$$

leads to an implicit relation for the pressure:

$$\frac{dp}{dz} = -\frac{p}{R_\mathrm{d} T_v} g. \tag{2.12}$$

2.5 Liquid water path

The liquid water path (LWP) is a measure of the total amount of liquid water between two points and is calculated by

$$\mathrm{LWP} = \int_0^h \rho_\mathrm{air} q_\mathrm{l} dz, \tag{2.13}$$

where $\rho_\mathrm{air} = \frac{p}{R_\mathrm{d} T_\mathrm{v}}$ according tot the gas law.

3 Physical processes of stratocumulus clouds

For the formation and maintenance of the stratocumulus, two conditions are essential. Firstly, a stable stratification in the free troposphere above the boundary layer is needed, such that deep convection is not allowed. Secondly, for the cloud formation a continuous supply of moisture is needed, which explains the frequent occurence over the oceans. A schematic overview of all the processes described in this chapter is provided in figure 3.1.

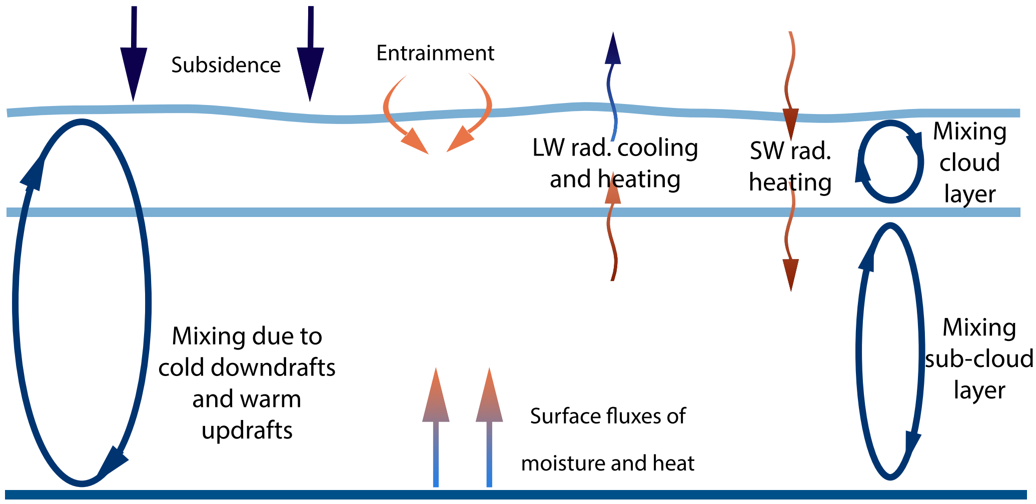

Figure 3.1 – Schematic cross-section of a boundary layer topped with a stratocumulus cloud. The physical processes that are important in the formation and maintenance of stratocumulus clouds are indicated.

3.1 Radiative forcing

Radiative forcing in stratocumulus is a main driver of turbulence. The radiation considered is splitted into two wavelength bands; shortwave (SW) and longwave (LW). This is possible because the peak in the solar spectrum is at the visible light wavelengths, while the earth is emitting infrared radiation and there are no other bodies near the earth that contribute significantly to the radiation budget [Stull, 1988].
A schematic overview of the longwave radiative flux is represented in figure 3.2. The downward longwave radiative flux from the atmosphere can be described by the Boltzmann equation:

$$F_{LW,\downarrow} = \epsilon_{\text{atm}} \sigma T_{\text{atm}}, \tag{3.1}$$

with σ the Stefan-Boltzmann constant, T_{atm} the temperature of the atmosphere and ϵ_{atm} the emissivity of the atmosphere, which is smaller than 1. In general stratocumulus clouds act approximately as a black body, for a cloud thickness larger than $\sim$ 100 m. The downward longwave radiative flux from the stratocumulus cloud can again be described by the Boltzmann equation, only with an emissivity ϵ_{cld} of approximately 1.

The emissivity of the sea surface can be approximated by $\epsilon_{\text{sea}} \approx 0.99$ [Sidran, 1981]. The cloud and surface emissivities are approximately the same. The surface temperature is only slightly larger than the cloud temperature and therefore the cloud base is slightly warmed. Because of this small temperature difference, the upward radiative flux is hardly affected by the presence of stratocumulus and is indicated with a straight line in figure 3.2.

The jump in the downward radiative flux, as can be seen in figure 3.2, creates a cooling effect in the top of the cloud layer. The net longwave radiative flux usually has a value of around 70 W/m^2, leading to a cooling rate of 5 to 10 K per hour.

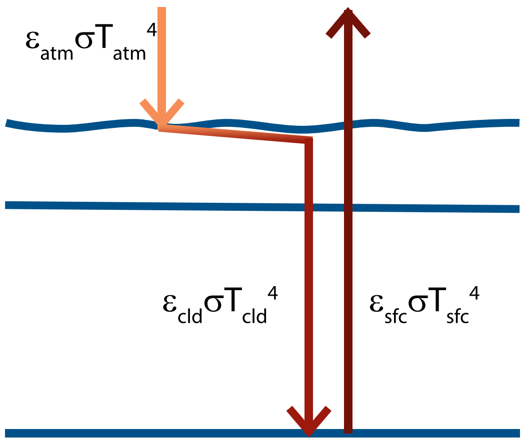

Figure 3.2 – Schematic cross-section of a boundary layer topped with a stratocumulus cloud, with an overview of the up- and downward longwave radiation.

Solar radiation also influences the cloud, but varies with time of the day, location, seasons and the presence of higher-level clouds. It is therefore harder to quantify. Incoming solar radiation is reflected, transmitted and absorbed by the stratocumulus. The relative amount of reflected solar radiation depends on the microphysical sructure of the cloud, but is typically 40 to 80 %. The amount of solar radiation absorbed by the cloud is in general less than 15 % and the rest is transmitted to the surface. The absorption of solar radiation leads to a warming of the cloud [van Zanten, 2000]. The absorbtion and transmission of the SW radiation is indicated by the red arrows in figure 3.1.

3.2 Entrainment and subsidence

Also crucial in the development of stratocumulus clouds is entrainment: the mixing of the air above the inversion into the boundary layer. At the top of the boundary layer the rising thermals hit the inversion layer where their vertical motion is damped. Because of their momentum, however, they overshoot and after that move downwards again due to their higher density than the surrounding air. During this descent warm dry air from above the inversion is dragged along and mixed into the boundary layer; a process called entrainment [Duynkerke et al., 1999]. The entrainment rate w_e defines the rate at which the boundary layer height grows and determines the magnitude of the warming and drying of the boundary layer [van Zanten, 2000]. It is therefore an important parameter for the evolution of the cloud, but it is difficult to measure [Stevens, 2003].
A counteracting process in the growth of the boundary layer is a large-scale subsiding motion, or subsidence. This subsidence is the downward branch of the Hadley-circulation, or the downward branch of an high pressure area.

3.3 Turbulent mixing

Turbulent mixing is an essential process in stratocumulus-topped boundary layers. In boundary layers without stratocumulus clouds, also called clear boundary layers, the turbulence is driven by convection from the earth surface. During the day, the sun warms the ground surface and the air close to the surface. Since warm air is less dense than cold air, the warm air close to the surface will rise. Such columns of rising air are called thermals. The rising thermals will mix with the surrounding air and therefore mix heat and moisture.
For stratocumulus-topped boundary layers, the stratocumulus clouds will block the sun, thereby reducing the surface solar radiation. The main cause for the mixing here is the longwave radiative effects at the cloud top [Lilly, 1968]. The air at the cloud top is locally cooled. The cool air starts to sink and creates turbulence. This mixing creates a vertically well-mixed boundary layer, with conserved variables q_t and θ_l that are nearly constant with height.

3.4 Decoupling and transition to cumulus

As air advects over warmer waters, the boundary layer deepens and decouples. The stratocumulus layer often exists within a mixed layers, called the cloud layer, but the eddies generated by the longwave cooling are not able to mix through the sub-cloud layer.

The sub-cloud layer, or near-surface layer, can still be mixed by the turbulence generated by the surface as in a clear boundary layer. The sub-cloud layer is therefore also a mixed layer.
Between the vertically well-mixed sub-cloud and cloud layer a transition layer is formed. The decoupling is accompanied by the development of cumulus on top of the sub-cloud layer and thinning of the stratocumulus layer [Wyant and Bretherton, 1997].

4 Mixed Layer Model

The mixed layer model (MLM) is a suitable tool to understand the effect of changes in different cloud controlling factors on the cloud amount. It considers the mixed layer (ML) in which conserved variables $\psi \in \{\theta_{\mathrm{l}}, q_{\mathrm{t}}\}$ are approximately constant with height because of intense vertical mixing [Stull, 1988]. In figure (4.1) a schematic representation of the mixed layer is shown, which starts at height $z = 0$ just above the sea surface and ends at the base of the inversion layer height z_{i}. The vertical profiles of conserved variables in the mixed layer are indicated with $q_{\mathrm{t,ML}}$ and $\theta_{\mathrm{l,ML}}$, q_t^+ and θ_{l}^+ are the values just above the inversion layer and $\theta_{\mathrm{l},0}$ and $q_{\mathrm{sat},0}$ are the surface values of q_{t} and θ_{l} respectively. The cloud base height z_{cb} is determined as the level where the total specific humidity q_{t} is equal to the saturation specific humidity q_{sat}.

To describe the conserved variables of the mixed layer, the vertically integrated

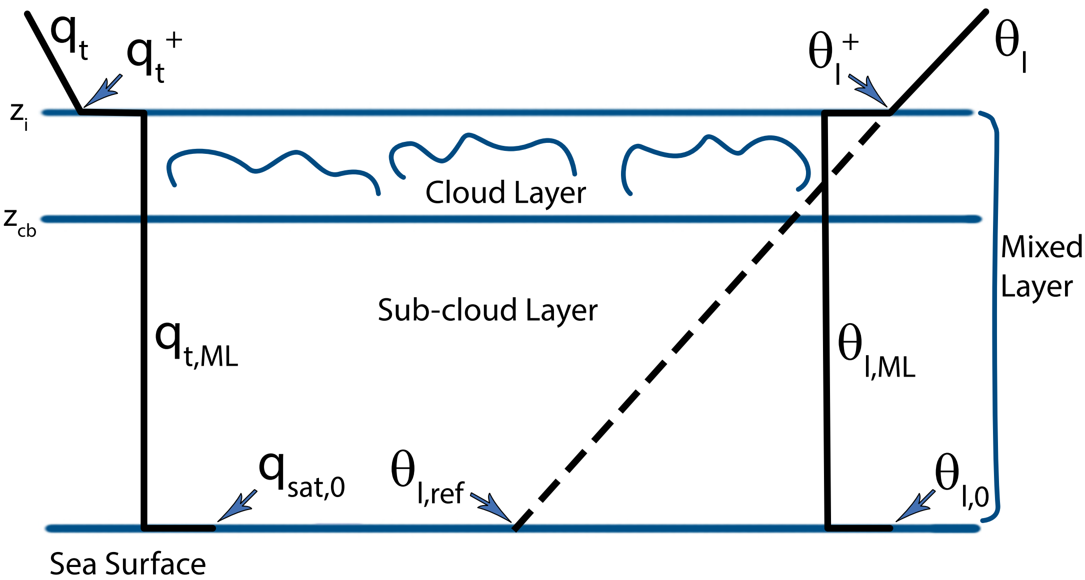

Figure 4.1 – Schematic representation of the mixed layer model. The mixed layer contains the cloud and sub-cloud layer. The vertical profiles of the conserved variables θ_{l} and q_{t} are indicated. The free tropospheric values are given by q_t^+ and θ_{l}^+, $q_{\mathrm{t,ML}}$ and $\theta_{\mathrm{l,ML}}$ indicate the mixed layer values and $q_{\mathrm{sat},0}$ and $\theta_{\mathrm{l},0}$ the surface values. The θ_{l}-profile in the free troposphere is related to the surface value $\theta_{\mathrm{l,ref}}$. The heights z_{i} and z_{cb} denote the inversion layer height and the cloud base height respectively.

budget equation for the conserved variables ψ is used:

$$z_{\mathrm{i}} \frac{\partial \psi_{\mathrm{ML}}}{\partial t} = F_{\psi,0} - F_{\psi,T} - \Delta S_{\psi}, \tag{4.1}$$

which can be qualitatively understood as the change of the conserved variables in the mixed layer (ψ_{ML}) by an inflow, outflow and a source/sink term. The derivation of the integrated budget equation can be found in section (B.2).
The values ψ_{ML} are governed by the turbulent flux at the surface $F_{\psi,0}$, at the top of the boundary layer $F_{\psi,T}$ and ΔS_{ψ} the total change of the source term between the surface and the top of the boundary layer. The latter can, for example, represent the effect of radiation.
The surface flux is obtained by using a bulk formula:

$$F_{\psi,0} = C_d U(\psi_0 - \psi_{\mathrm{ML}}), \tag{4.2}$$

with U the horizontal wind speed at the surface.
The flux at the top is proportional to the entrainment rate w_{e} and the jump of ψ across the inversion:

$$F_{\psi,T} = -w_{\mathrm{e}}(\psi^{+} - \psi_{\mathrm{ML}}), \tag{4.3}$$

[Lilly, 1968]. The values ψ^{+} are just above the inversion layer, which is considered to have a very small thickness.
Substituting the surface and top fluxes into equation (4.1) gives:

$$z_{\mathrm{i}}\frac{\partial \psi_{\mathrm{ML}}}{\partial t} = C_d U(\psi_0 - \psi_{\mathrm{ML}}) + w_{\mathrm{e}}(\psi^{+} - \psi_{\mathrm{ML}}) - \Delta S_{\psi}. \tag{4.4}$$

To complete the MLM, the boundary layer height z_i is needed. The inversion layer height grows because of entrainment, the mixing of warm and dry air into the boundary layer, but is counteracted by the subsidence, which is a mean vertical motion pushing on the boundary layer. The tendency of z_{i} is therefore given by:

$$\frac{\partial z_{\mathrm{i}}}{\partial t} = w_{\mathrm{e}} + \overline{w}. \tag{4.5}$$

Here $\overline{w}$ represents the large-scale subsidence velocity.

4.1 Boundary conditions

To solve the MLM equations, boundary conditions at height z_{i}^{+}, just above the inversion layer, are required. For the free troposphere the variation of the potential temperature is given by

$$\theta_{\mathrm{l}}(z) = \theta_{\mathrm{l,ref}} + \Gamma_{\theta} z, \tag{4.6}$$

with lapse rate $\Gamma_{\theta} = 6$ K km^{-1} and $\theta_{\mathrm{l,ref}}$ the value of the potential temperature in the free troposphere extrapolated to the surface. The specific humidity in the free troposphere is taken constant such that no saturation occurs, usually $0 \leq q_{t,ft} \leq 10$ g kg^{-1}.

The subsidence at the inversion layer height z_i is hard to measure, but can be estimated if the large-scale divergence of the horizontal wind is known as a function of height. Assuming the divergence does not depend on height, the subsidence reads:

$$\overline{w}(z_\mathrm{i}) = -\int_{z=0}^{z_\mathrm{i}} \left(\frac{\partial \overline{u}}{\partial x} + \frac{\partial \overline{v}}{\partial y} \right) dz = -\int_{z=0}^{z_\mathrm{i}} D(z) dz = -D z_\mathrm{i}, \tag{4.7}$$

with u and v the horizontal wind velocities [Stull, 1988, de Roode et al., 2012].

The drizzle source term ΔS_{q_t} is set to zero. This is particularly applicable for a polluted environment in which clouds have a high droplet concentration and small drizzle fluxes. In the source term of the liquid water potential temperature, the radiative forcing is included, which has a cooling effect at the cloud top:

$$\Delta S_{\theta_\mathrm{l}} = \frac{\Delta F_{rad}}{\rho_{air} c_p} = \Delta F. \tag{4.8}$$

The entrainment rate can be obtained from a ratio of a measure of buoyancy forcing to a measure of the inversion stability. For the entrainment rate different parameterisations have been developed from LES results and several are discussed by Stevens [2003]. De Roode et al. [2012] used the parameterisation by Nicholls and Turton in their MLM-studies, which can be written as:

$$w_\mathrm{e} = A \frac{w_*^3}{z_\mathrm{i} \Delta b}, \tag{4.9}$$

with A the entrainment efficiency and

$$\Delta b \approx \frac{g}{\theta_0} \Delta \theta_\mathrm{v} \tag{4.10}$$

the buoyancy jump over the inversion, with g the acceleration due to gravity. The velocity scale w_* is a function of the vertical integral of the buoyancy flux:

$$w_* = \left(2.5 \frac{g}{\theta_0} \int_0^{z_\mathrm{i}} \overline{w' \theta_\mathrm{v}'} dz \right)^{\frac{1}{3}}, \tag{4.11}$$

[Turton and Nicholls, 1987]. The Nicholls and Turton parameterisation is not trivial to apply in a two-layer model as it depends on the buoyancy flux throughout the whole mixed layer. In the two-layer model the cloud and sub-cloud layer are coupled through a transition layer, in which the buoyancy flux is not known.

Throughout this research therefore another parameterisation is applied, used in earlier research from Dal Gesso et al. [2014b]:

$$w_e = \eta \frac{\Delta F}{\Delta \theta_\mathrm{l}}, \tag{4.12}$$

with efficiency factor η and $\Delta\theta_l$ the liquid potential temperature inversion jump: $\Delta\theta_\mathrm{l} = \theta_\mathrm{l}(z_\mathrm{i}^+) - \theta_{\mathrm{l,ML}}$. The efficiency factor used by Dal Gesso et al. is $\eta = 0.7$.

4.2 Steady-state solutions

Steady-state solutions are easier to obtain than transient solutions since time as a variable is removed. In a steady-state solution, the entrainment rate balances the subsidence, as can easily be seen from equation (4.5):

$$w_\mathrm{e} = -\overline{w} = Dz_\mathrm{i}. \tag{4.13}$$

A steady-state solution for $\theta_{\mathrm{l,ML}}$ is found by combining the entrainment parameterisation of equation (4.12) and the heat equation (4.4):

$$\theta_{\mathrm{l,ML}} = \theta_{\mathrm{l,0}} - \frac{(1-\eta)\Delta F}{C_D U}. \tag{4.14}$$

An expression for $q_{\mathrm{t,ML}}$ is obtained from combining the budget equation (4.4) and equation (4.13):

$$q_{\mathrm{t,ML}} = q_{\mathrm{t,0}} + \frac{Dz_\mathrm{i}(q_t^+ - q_{\mathrm{t,0}})}{C_d U + Dz_\mathrm{i}}. \tag{4.15}$$

The inversion layer height z_i follows from equation (4.13) and the entrainment parameterisation from equation (4.12):

$$z_\mathrm{i} = \frac{\eta \Delta F}{\Delta\theta_\mathrm{l} D}. \tag{4.16}$$

5 Two-layer model

The MLM assumes a well-mixed layer, with constant variables ψ that are the same in the sub-cloud and the cloud layer. However, observations show that the boundary layer does not remain well-mixed when it deepens [Nicholls, 1984, Albrecht, 1995, Betts, 1995]. The key process in the transition from stratocumulus to cumulus clouds is entrainment. Entrainment of free-tropospheric air into the stratocumulus-topped boundary layer (STBL) leads to deepening, which makes it increasingly difficult to sustain the mixing throughout the whole boundary layer [Nicholls and Leighton, 1985]. The eddies in the cloud layer become distinct from those in the sub-cloud layer and the STBL begins to separate into two layers: a cloud layer and a sub-cloud layer [Rogers and Koracin, 1992]. The BL is then said to be decoupled. The distinct eddies still mix the sub-cloud and the cloud layer separately, creating two mixed layers on top of each other. Cumulus clouds start to form at the top of the sub-cloud layer [Bretherton and Wyant, 1997, Park et al., 2004].

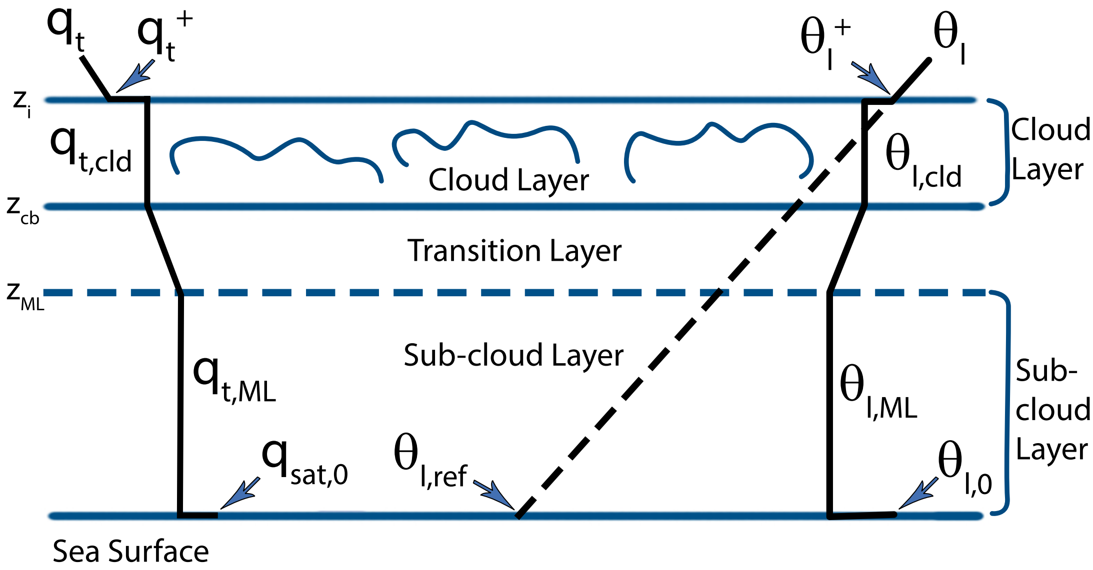

Figure 5.1 – Schematic representation of the two-layer model. The two mixed layers, the cloud and sub-cloud layer are connected through the transition layer. The sub-cloud layer starts at the surface and ends at the sub-cloud layer height z_{ML}. The cloud layer starts at the cloud base height z_{cb} up to the inversion layer height z_{i}. In the cloud layer the conserved variables are $\theta_{\mathrm{l,cld}}$ and $q_{\mathrm{t,cld}}$ and in the sub-cloud layer the conserved variables are $\theta_{\mathrm{l,ML}}$ and $q_{\mathrm{t,ML}}$. The conserved variables in the transition layer are unknown and assumed to vary linaerly with height.

In the decoupled BL the conserved variables ψ are no longer the same in the cloud and sub-cloud layer, but are still constant with height in each individual layer due to vertical mixing within each layer. To describe such a decoupled BL a two-layered mixed layer model is used, that will be referred to as 'two-layer model'. A sketch of the profiles of conserved variables q_t and θ_l is shown in figure 5.1. In this figure both the cloud layer and sub-cloud layer with different q_t and θ_l are shown, where the cloud variables are indicated with $q_{t,cld}$ and $\theta_{l,cld}$ and the sub-cloud layer variables with $q_{t,ML}$ and $\theta_{l,ML}$. The notation for the sub-cloud layer variables $q_{t,ML}$ and $\theta_{l,ML}$ might be somewhat confusing as it is the same notation as used in the MLM for the mixed-layer variables and it refers only to the sub-cloud layer as a mixed layer, while the cloud layer is also a mixed layer. This notation has been chosen nevertheless as it is the same as used in earlier work about decoupled boundary layers from Park et al. [2004].

The transition between the cloud layer and sub-cloud layer takes place in the transition layer. The exact profile inside this transition layer is unknown, but is here estimated as a linear interpolation between the cloud and sub-cloud variables.

To describe the boundary layer multiple variables are required. The variables q_t and θ_l in both mixed layers are wanted, which determine the height of the sub-cloud layer and the cloud base. To determine the thickness of the cloud also the inversion layer height z_i is necessary. The inversion layer height is still determined by equation (4.5). To obtain q_t and θ_l the integrated budget equations are used, for which the derivation can be found in section B.2. The budget equations for the cloud, transition and sub-cloud layer are:

$$\frac{\partial \psi_{\mathrm{cld}}}{\partial t} = \frac{w_e \Delta\psi - \Delta S_{\mathrm{cld}} + F_{\psi,z_{\mathrm{cb}}}}{z_{\mathrm{cld}}} \tag{5.1}$$

$$\frac{\partial \psi_{\mathrm{tr}}}{\partial t} = \frac{-F_{\psi,z_{\mathrm{cb}}} + F_{\psi,z_{\mathrm{ML}}} - \Delta S_{\mathrm{tr}}}{z_{\mathrm{cb}} - z_{\mathrm{ML}}}. \tag{5.2}$$

$$\frac{\partial \psi_{\mathrm{sub}}}{\partial t} = \frac{-F_{\psi,z_{\mathrm{ML}}} - \Delta S_{\mathrm{ml}} + F_{\psi,0}}{z_{\mathrm{ML}}}, \tag{5.3}$$

with ΔS the source term over the entire cloud or sub-cloud layer and cloud thickness $z_{\mathrm{cld}} = z_i - z_{\mathrm{cb}}$. In the three equations (5.1), (5.2) and (5.3) there are five unknowns: ψ_{cld}, ψ_{tr}, ψ_{ML}, $F_{\psi,z_{\mathrm{ML}}}$ and $F_{\psi,z_{\mathrm{cb}}}$. To get to a closure of the system, ψ_{cld} and ψ_{ML} are required to obey the relation found by Park et al. [2004]:

$$\psi_{\mathrm{cld}} = \psi_{\mathrm{ML}} + \alpha_\psi(\psi^+ - \psi_{\mathrm{ML}}), \tag{5.4}$$

where $\alpha_\psi \in (\alpha_\theta, \alpha_q)$ represents the so-called decoupling parameter. Following the paper of Park et al., Wood and Bretherton [2004] did an observational study and found that α_ψ could be well fit by:

$$\alpha_\psi = r_\psi(z_\mathrm{i} - z_\mathrm{ML}), \tag{5.5}$$

with z_ML the height of the sub-cloud layer.

5.1 Steady-state solution

The four equations (5.1), (5.2), (5.3) and (5.4) can be used to obtain the steady state of the boundary layer. As the changes over time are zero in steady state, ψ_tr drops out of the equations leaving four equations and four unknowns: ψ_cld, ψ_ML, F_{ψ,z_ML} and F_{ψ,z_cb}.
No precipitation is taken into account and the radiative cooling takes place over a relatively thin layer and is therefore only considered in the cloud budget equation [Garrat, 1994]. With the fluxes at the top and surface known, the fluxes at z_cb and z_ML are wanted. From equation 5.2 it follows that they are related to each other by $F_{\psi,z_\mathrm{ML}} = F_{\psi,z_\mathrm{cb}}$. To express the fluxes F_{ψ,z_ML} and F_{ψ,z_cb} in known variables, equations 5.3 and 4.2 are combined to:

$$F_{\psi,z_\mathrm{ML}} = F_{\psi,z_\mathrm{cb}} = F_{\psi,0} = C_d U\left(\psi_0 - \psi_\mathrm{ML}\right). \tag{5.6}$$

The only unknowns left are ψ_cld and ψ_ML. The first expression that can be used to solve $\theta_\mathrm{l,ML}$ is equation (5.6). A second expression for F_{ψ,z_ML} can be obtained from equation (5.1):

$$F_{\theta_\mathrm{l},z_\mathrm{cb}} = -w_\mathrm{e}\left(\theta_\mathrm{l}^+ - \theta_\mathrm{l,cld}\right) + \Delta F. \tag{5.7}$$

Combining these equations (5.6) and (5.7) and rewriting to solve $\theta_\mathrm{l,ML}$ results in:

$$\theta_\mathrm{l,ML} = \theta_\mathrm{l,0} + \frac{w_\mathrm{e}\left(\theta_\mathrm{l}^+ - \theta_\mathrm{l,cld}\right) - \Delta F}{C_d U}, \tag{5.8}$$

which still contains two unknowns: $\theta_\mathrm{l,ML}$ and $\theta_\mathrm{l,cld}$. To eliminate $\theta_\mathrm{l,cld}$, the entrainment parameterisation from equation 4.12 can be used. The θ_l-jump over the inversion layer is then substituted into equation (5.8) to obtain:

$$\theta_\mathrm{l,ML} = \theta_\mathrm{l,0} - \frac{(1-\eta)\,\Delta F}{C_d U}. \tag{5.9}$$

Now that $\theta_\mathrm{l,ML}$ is known, $\theta_\mathrm{l,cld}$ can be calculated using equation (5.4). The liquid water potential temperature in the sub-cloud layer does not depend on the rate of decoupling, but $\theta_\mathrm{l,cld}$ does. If the decoupling is very small:

$$\lim_{\alpha_\theta \to 0} \theta_\mathrm{l,cld} = \theta_\mathrm{l,ML}, \tag{5.10}$$

since the two-layer model without decoupling reduces to the MLM. For very large decoupling:

$$\lim_{\alpha_\theta \to 1} \theta_{\mathrm{l,cld}} = \theta_{\mathrm{l}}^{+}, \tag{5.11}$$

where the cloud layer liquid potential temperature is pushed towards the free tropospheric θ_{l}.
The remaining variables that need to be calculated are $q_{\mathrm{t,ML}}$ and $q_{\mathrm{t,cld}}$. To solve $q_{\mathrm{t,ML}}$ the same strategy is used as for $\theta_{\mathrm{l,ML}}$, with the only difference that there are no source terms for q_{t}. A first equation used to solve $q_{\mathrm{t,ML}}$ is (5.6). A second expression for $F_{q_{\mathrm{t}},z_{\mathrm{cb}}}$ can be found again from equation (5.1):

$$F_{q_{\mathrm{t}},z_{\mathrm{cb}}} = -w_{\mathrm{e}} \left(q_t^{+} - q_{\mathrm{t,cld}} \right). \tag{5.12}$$

Combining equations (5.6) and (5.12) and rewriting leads to an expression for $q_{\mathrm{t,ML}}$:

$$q_{\mathrm{t,ML}} = q_{\mathrm{t,0}} + \frac{w_{\mathrm{e}} \left(q_t^{+} - q_{\mathrm{t,cld}} \right)}{C_d U}, \tag{5.13}$$

which still contains two unknowns: $q_{\mathrm{t,ML}}$ and $q_{\mathrm{t,cld}}$. Here the entrainment parameterisation cannot be used to solve $q_{\mathrm{t,ML}}$, as the equation involves the q_{t}-jump instead of the θ_{l}-jump. A second equation containing both $q_{\mathrm{t,ML}}$ and $q_{\mathrm{t,cld}}$ was stated in equation (5.4). Combining equations (5.4) and (5.13) results in:

$$q_{\mathrm{t,ML}} = \frac{q_{\mathrm{t,0}} + \frac{w_{\mathrm{e}}}{C_d U} \left(1 - \alpha_q\right) q_t^{+}}{1 + \frac{w_{\mathrm{e}}}{C_d U} \left(1 - \alpha_q\right)} = \frac{C_d U q_{\mathrm{t,0}} + D z_{\mathrm{i}} \left(1 - r_q \left(z_{\mathrm{i}} - z_{\mathrm{ML}}\right)\right) q_t^{+}}{C_d U + D z_{\mathrm{i}} \left(1 - r_q \left(z_{\mathrm{i}} - z_{\mathrm{ML}}\right)\right)}, \tag{5.14}$$

where equations (4.12) and (5.5) are used to substitute w_{e} and α_q. Now that $q_{\mathrm{t,ML}}$ is known, equation (5.4) can be used to obtain $q_{\mathrm{t,cld}}$. The total specific humidity in the sub-cloud and cloud layer depends on the rate of decoupling. If the decoupling is very small:

$$\begin{aligned} \lim_{\alpha_q \to 0} q_{\mathrm{t,ML}} &= q_{\mathrm{t,0}} + \frac{D z_{\mathrm{i}} (q_t^{+} - q_{\mathrm{t,0}})}{C_d U + D z_{\mathrm{i}}}, \\ \lim_{\alpha_q \to 0} q_{\mathrm{t,cld}} &= q_{\mathrm{t,ML}}, \end{aligned} \tag{5.15}$$

giving the same solution as the steady state solution from the MLM in equation 4.15, since the two-layer model without decoupling reduces to the MLM. For very large decoupling

$$\begin{aligned} \lim_{\alpha_q \to 1} q_{\mathrm{t,ML}} &= q_{\mathrm{t,0}}, \\ \lim_{\alpha_q \to 1} q_{\mathrm{t,cld}} &= q_t^{+}, \end{aligned} \tag{5.16}$$

where the humidity state of the sub-cloud layer is pushed towards the surface humidity $q_{\mathrm{t},0}$ and the cloud layer is pushed towards the free tropospheric humidity. When observing equations (5.4) and (5.14) is becomes clear that to calculate $q_{\mathrm{t,ML}}$, $q_{\mathrm{t,cld}}$ and $\theta_{\mathrm{l,cld}}$ the inversion layer height z_{i} is needed and should be calculated. To obtain a relation for z_{i}, equations (5.4) and (5.14) are used:

$$r_\theta(z_{\mathrm{i}} - z_{\mathrm{ML}}) = 1 - \frac{\Delta\theta_{\mathrm{l}}}{\theta_{\mathrm{l}}^{+} - \theta_{\mathrm{l,ML}}}, \tag{5.17}$$

where $\theta_{\mathrm{l,ML}}$ depends on z_{i} and can be removed from the equation by substituting equation (5.9) into equation (5.17). Rearranging after this substitution gives:

$$\left[r_\theta\left(z_{\mathrm{i}} - z_{\mathrm{ML}}\right) - 1\right]\left[\theta_{\mathrm{l}}^{+} - \theta_{\mathrm{l},0} + \frac{(1-\eta)\,\Delta F}{C_d U}\right] + \Delta\theta_{\mathrm{l}} = 0. \tag{5.18}$$

The θ_{l}-jump depends on $\theta_{\mathrm{l,cld}}$ and therefore on z_{i}. To eliminate $\Delta\theta_{\mathrm{l}}$ from equation (5.18), the entrainment parameterisation from (4.12) is rewritten to obtain:

$$\Delta\theta_{\mathrm{l}} = \frac{\eta\Delta F}{w_{\mathrm{e}}} = \frac{\eta\Delta F}{D z_{\mathrm{i}}}, \tag{5.19}$$

where $w_{\mathrm{e}} = -\overline{w} = D z_{\mathrm{i}}$ according to the steady-state solution of equation (4.5) and the subsidence equation from equation (4.7). The substitution of equation (4.6) and (5.19) into equation (5.18) eliminates the last variables that depend on z_{i}. This results in the equation:

$$z_{\mathrm{i}}\left[r_\theta\left(z_{\mathrm{i}} - z_{\mathrm{ML}}\right) - 1\right]\left[\theta_{\mathrm{l,ref}} + \Gamma_\theta z_{\mathrm{i}} - \theta_{\mathrm{l},0} + \frac{(1-\eta)\,\Delta F}{C_d U}\right] + \frac{\eta\Delta F}{D} = 0 \tag{5.20}$$

that still involves one unknown: the sub-cloud layer height z_{ML} where such a relative humidity (RH) is reached that condensation starts to occur. The RH-profile in the sub-cloud layer is determined by $q_{\mathrm{t,ML}}$ and $\theta_{\mathrm{l,ML}}$, which cannot be calculated before calculating z_{i}. In order to obtain an analytical solution, the approximation

$$\alpha_\psi = r_\psi\left(z_{\mathrm{i}} - z_{\mathrm{ML}}\right) \approx r_\psi z_{\mathrm{i}} \tag{5.21}$$

is used. This results in the polynomial

$$\begin{aligned} z_{\mathrm{i}}^3 r_\theta \Gamma_\theta + z_{\mathrm{i}}^2 &\left\{ r_\theta \left[\theta_{\mathrm{l,ref}} - \theta_{\mathrm{l},0} + \frac{(1-\eta)\,\Delta F}{C_d U}\right] - \Gamma_\theta \right\} \\ &+ z_{\mathrm{i}}\left[-\theta_{\mathrm{l,ref}} + \theta_{\mathrm{l},0} - \frac{(1-\eta)\,\Delta F}{C_d U}\right] + \frac{\eta\Delta F}{D} = 0, \end{aligned} \tag{5.22}$$

that can be solved for z_{i}. The cloud base height is determined as the height in the cloud layer where condensation starts to occur. For this q_{sat} is calculated with equation (2.9) and $\theta_{\mathrm{l,cld}}$. Then $q_{\mathrm{t,cld}}$ is compared with q_{sat} to determine the cloud base height.

5.2 Transient Solutions

The four equations (5.1), (5.2), (5.3) and (5.4) with the five unknowns ψ_{cld}, ψ_{tr}, ψ_{ML}, $F_{\psi,z_{\mathrm{ML}}}$ and $F_{\psi,z_{\mathrm{cb}}}$ are used to obtain the transient solutions of the two-layer model. To close the problem, a fifth equation is needed.

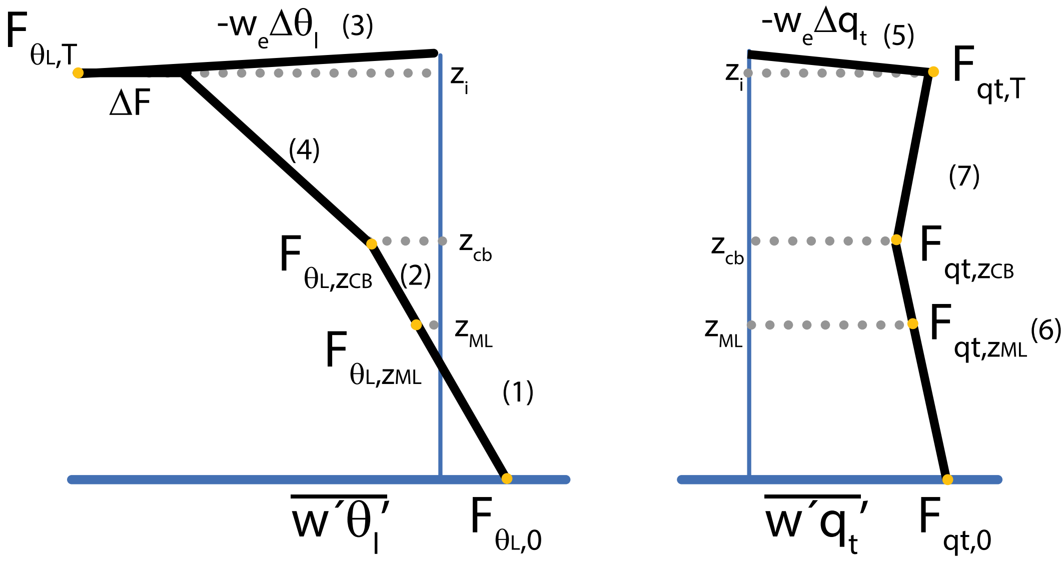

Figure 5.2 – Schematic overview of the heat and moisture fluxes in a decoupled boundary layer. The numbers indicate the steps taken to obtain all the information needed to describe the evolution of the boundary layer. The explanation of all steps can be found in the text.

In figure 5.2 a schematic procedure of the steps in this section is shown. The steps in the text corresponding to the steps in the figure are indicated with **(n)**, where n is the number of the step.
A fifth equation is obtained by relating the flux at the top of the sub-cloud layer to the flux at the surface by:

$$F_{\psi,z_{\mathrm{ML}}} = f_\psi F_{\psi,0}, \tag{5.23}$$

with flux ratio f_ψ **(1)**. From LES results and observations the ratio for the θ_{v}-flux is found to be approximately $f_{\theta_{\mathrm{v}}} = -0.25$. To obtain $f_{\theta_{\mathrm{l}}}$ it can be used that for clear air

$$\overline{w'\theta_{\mathrm{v}}'} \approx A_d\overline{w'\theta_{\mathrm{l}}'} + B_d\overline{w'q_{\mathrm{t}}'}, \tag{5.24}$$

with $Ad \approx 1.01$ and $B_d \approx 0.608\theta_{\mathrm{ml}}$ [de Roode et al., 2004]. It then follows that

$$f_{\theta_{\mathrm{l}}} = f_{\theta_{\mathrm{v}}} + \frac{B_d F_{q_{\mathrm{t}},0}\left(f_{\theta_{\mathrm{v}}} - f_{q_{\mathrm{t}}}\right)}{A_d F_{\theta_{\mathrm{l}},0}}, \tag{5.25}$$

where from LES results of stratocumulus transition cases $f_{q_t} = 0.9$ is suggested by van der Dussen et al. [2013]. Since the fluctuation of the humidity flux ratio over a diurnal cycle is a larger than the fluctuation of f_{θ_l}, f_{q_t} is only used to obtain f_{θ_l} and the flux $F_{q_t,z_{\mathrm{ML}}}$ is not fixed with this ratio as in equation (5.23).

A first attempt to close the problem did not succeed. The prescribed entrainment parameterisation from equation (4.12) led to a top flux for which $F_{\theta_l,T} + \Delta F > 0$. The decoupling restriction requires the cloud layer to warm faster than the sub-cloud layer, resulting in an even larger $F_{\theta_l,z_{\mathrm{cb}}}$, as shown in figure 5.3. According to equation (5.23) the flux at the top of the sub-cloud layer $F_{\theta_l,z_{\mathrm{ML}}}$ is however negative. The flux profile in the transition layer is determined by $F_{\theta_l,z_{\mathrm{ML}}}$ and $F_{\theta_l,z_{\mathrm{cb}}}$. This flux profile then indicates that both cloud and sub-cloud layer are then warming, while the transition layer is rapidly cooling, which is very unrealistic.

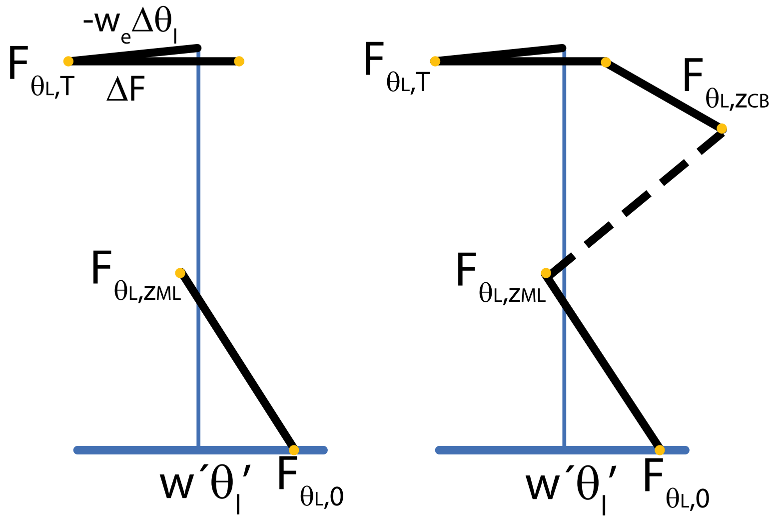

Figure 5.3 – A schematic overview of the heat flux in a decoupled boundary layer. The left profile indicates the first steps taken, where the flux profile on the right is completed. This flux profile was obtained in a first attempt to obtain a solution for the evolution of the boundary layer. It indicates the warming of the cloud and sub-cloud layer and the cooling of the transient layer, which is very unrealistic.

To avoid the transition layer from cooling while the rest of the boundary layer is warming, a linear flux profile has been chosen between the surface and the stratocumulus cloud base and the entrainment rate has not been fixed according to equation (4.12). The transition layer now follows the same tendency as the sub-cloud layer. A linear flux profile between z_{ML} and z_{i} would also have been a possibility, the transition layer would then follow the same tendency as the cloud layer.

The first unknown to solve is $\theta_{\mathrm{l,ML}}$. According to equation (5.3) the evolution of $\theta_{\mathrm{l,ML}}$ depends on the fluxes at the surface and at z_{ML}. The flux at the surface is known from equation (4.2) and the flux at z_{ML} is known from equation (5.23), so the tendency of $\theta_{\mathrm{l,ML}}$ is known and can be rewritten as:

$$\frac{\partial \theta_{\mathrm{l,ML}}}{\partial t} = \frac{F_{\theta_{\mathrm{l}},0}\left(1 - f_{\theta_{\mathrm{l}}}\right)}{z_{\mathrm{ML}}}. \tag{5.26}$$

To obtain the tendency of $\theta_{\mathrm{l,cld}}$ the fluxes at z_{cb} and the top are needed according to equation (5.1). Since a linear flux profile between the surface and the cloud base is assumed, the flux at z_{cb} can be written as:

$$F_{\theta_{\mathrm{l}},z_{\mathrm{cb}}} = F_{\theta_{\mathrm{l}},0}\left[1 + \frac{z_{\mathrm{cb}}}{z_{\mathrm{ML}}}\left(f_{\theta_{\mathrm{l}}} - 1\right)\right], \tag{5.27}$$

(2). The top flux, however, depends on the entrainment rate according to:

$$F_{\psi,T} = -w_{\mathrm{e}}\left(\psi^{+} - \psi_{\mathrm{cld}}\right). \tag{5.28}$$

Therefore an entrainment rate should be found such that the cloud layer and sub-cloud layer are (de)coupled via equation (5.4) and such that the transition layer has the same tendency as the sub-cloud layer. To obey the decoupling of the cloud and sub-cloud layer the derivative of equation (5.4) with respect to time is used as a starting point:

$$\frac{\partial \theta_{\mathrm{l,cld}}}{\partial t} = \alpha_{\theta}\frac{\partial \theta_{\mathrm{l}}^{+}}{\partial t} + \left(1 - \alpha_{\theta}\right)\frac{\partial \theta_{\mathrm{l,ML}}}{\partial t}. \tag{5.29}$$

The time derivative of α_{θ} is neglected. The time derivative of α_{θ} reads: $\frac{\partial \alpha_{\theta}}{\partial t} = r_{\theta}\left(\frac{\partial z_{\mathrm{i}}}{\partial t} - \frac{\partial z_{\mathrm{ML}}}{\partial t}\right)$, where the growth of z_{i} and the growth of z_{ML} oppose each other such that the tendency of α_{θ} is diminished. The tendency of the free tropospheric values is given by:

$$\frac{\partial \theta_{\mathrm{l}}^{+}}{\partial t} = w_{\mathrm{e}}\left(\frac{\partial \theta_{\mathrm{l}}}{\partial z}\right)_{\text{free troposphere}} = w_{\mathrm{e}}\Gamma_{\theta}. \tag{5.30}$$

Equations (5.1), (5.26) and (5.30) are substituted into equation (5.29) to obtain a relation for the entrainment rate w_{e}:

$$\frac{w_{\mathrm{e}}\Delta\theta_{\mathrm{l}} - \Delta F + F_{\theta_{\mathrm{l}},z_{\mathrm{cb}}}}{z_{\mathrm{cld}}} = \alpha_{\theta} w_{\mathrm{e}}\Gamma_{\theta} + \left(1 - \alpha_{\theta}\right)\frac{F_{\theta_{\mathrm{l}},0}\left(1 - f_{\theta_{\mathrm{l}}}\right)}{z_{\mathrm{ML}}}. \tag{5.31}$$

The entrainment rate now already obeys the decoupling between the cloud and sub-cloud layer. To make sure that the transition layer has the same tendency as the sub-cloud layer equation (5.27) is substituted in equation (5.31). Rearranging gives an expression for w_e:

$$w_\mathrm{e} = \frac{F_{\theta_\mathrm{l},0}\left\{1 + \frac{(f_{\theta_\mathrm{l}}-1)}{z_\mathrm{ML}}\left[z_\mathrm{i}\left(1-\alpha_\theta\right) + \alpha_\theta z_\mathrm{cb}\right]\right\} - \Delta F}{\alpha_\theta \Gamma_\theta z_\mathrm{cld} - \Delta\theta_\mathrm{l}}. \tag{5.32}$$

Now that the entrainment rate is known, also the top flux $F_{\theta_\mathrm{l},T}$ from equation (5.28) can be calculated **(3)**. Using this flux and $F_{\theta_\mathrm{l},z_\mathrm{cb}}$ from equation (5.27) in equation (5.1) fixes the tendency of $\theta_\mathrm{l,cld}$ **(4)**.
The profile of q_t is now still unknown. To obtain the tendency of $q_\mathrm{t,cld}$ the fluxes at the top and at the stratocumulus cloud base are required according to equation (5.1). The top flux $F_{q_\mathrm{t},T}$ can be calculated according to (5.28) now that the entrainment rate is known **(5)**. Since the fluxes are assumed linear from the surface to the stratocumulus cloud base, a relation for the flux $F_{q_\mathrm{t},z_\mathrm{cb}}$ is obtained:

$$F_{q_\mathrm{t},z_\mathrm{cb}} = \frac{z_\mathrm{cb}}{z_\mathrm{ML}}\left(F_{q_\mathrm{t},z_\mathrm{ML}} - F_{q_\mathrm{t},0}\right) + F_{q_\mathrm{t},0}, \tag{5.33}$$

which ensures that the tendency of the transient layer is equal to the tendency of the sub-cloud layer. This flux however depends on the flux $F_{q_\mathrm{t},z_\mathrm{ML}}$, which is still unknown. Since the flux ratio f_{q_t} is not fixed, as explained before, $F_{q_\mathrm{t},z_\mathrm{ML}}$ cannot be calculated in the same way as $F_{\theta_\mathrm{l},z_\mathrm{ML}}$. The vertical profile of q_t should also obey the decoupling equation (5.4) and therefore this equation is used to obtain a second equation with the two unknowns $F_{q_\mathrm{t},z_\mathrm{cb}}$ and $F_{q_\mathrm{t},z_\mathrm{ML}}$. The time derivative of equation (5.4) is taken and equations (5.1), (5.3) and (5.30) are substituted for the tendencies of $q_\mathrm{t,cld}$, $q_\mathrm{t,ML}$ and q_t^+ respectively:

$$\frac{-F_{q_\mathrm{t},T} + F_{q_\mathrm{t},z_\mathrm{cb}}}{z_\mathrm{cld}} = \alpha_q w_\mathrm{e} \Gamma_q + \left(1-\alpha_q\right)\frac{\left(-F_{q_\mathrm{t},z_\mathrm{ML}} + F_{q_\mathrm{t},0}\right)}{z_\mathrm{ML}}. \tag{5.34}$$

Combining the two equations (5.33) and (5.34) with the two unknowns gives an expression for the flux at the sub-cloud layer height:

$$F_{q_\mathrm{t},z_\mathrm{ML}} = F_{q,0} + \frac{z_\mathrm{ML}\left(F_{q_\mathrm{t},T} + \alpha_q z_\mathrm{cld} w_\mathrm{e} \Gamma_{q_\mathrm{t}} - F_{q,0}\right)}{z_\mathrm{i} - \alpha_q z_\mathrm{cld}}, \tag{5.35}$$

(6). Now that the fluxes at the surface and z_ML are fixed, the tendency of $q_\mathrm{t,ML}$ can be calculated according to equation (5.3). The flux at $F_{q_\mathrm{t},z_\mathrm{cb}}$ is found according to equation (5.33), using the known $F_{q_\mathrm{t},z_\mathrm{ML}}$ **(7)**. With $F_{q_\mathrm{t},z_\mathrm{cb}}$ and $F_{q_\mathrm{t},T}$ the tendency of $q_\mathrm{t,cld}$ is fixed according to equation (5.1).
Now that the vertical profiles of θ_l and q_t are known and the inversion layer height is calculated according to equation (4.5), only the new z_cb and z_ML are needed.

The new vertical profiles of θ_{l} and q_{t} result in a new relative humidity profile. The height at which the RH reaches a critical point and condensation starts to occur will therefore be different with the new vertical profiles of θ_{l} and q_{t}. This effect and subsidence prescribe the change of both z_{ML} and z_{cb}:

$$\frac{\partial z_{\mathrm{ML}}}{\partial t} = \frac{\partial z_{\mathrm{ML}}\left(\mathrm{RH} = \mathrm{RH}_{\mathrm{crit}}\right)}{\partial t} + \overline{w}\mid_{z_{\mathrm{ML}}}, \tag{5.36}$$

where a RH criterion $\mathrm{RH}_{\mathrm{crit}}$is set to slightly less than unity. The change of z_{cb} is given by:

$$\frac{\partial z_{\mathrm{cb}}}{\partial t} = \frac{\partial z_{\mathrm{cb}}\left(\mathrm{RH} = 1\right)}{\partial t} + \overline{w}\mid_{z_{\mathrm{cb}}}, \tag{5.37}$$

where the cloud base is determined by the level at which the air is just saturated. The new heights of the layers are acquired. When considering these new heights and assuming that θ_{l} and q_{t} in the cloud and sub-cloud layers do not change, the values in the transition layer should change. This can be seen by considering budget equation for the whole boundary layer, that consists of equations (5.1), (5.2) and (5.3):

$$z_{\mathrm{cld}}\frac{\partial \psi_{\mathrm{cld}}}{\partial t} + \left(z_{\mathrm{cb}} - z_{\mathrm{ML}}\right)\frac{\partial \psi_{\mathrm{tr}}}{\partial t} + z_{\mathrm{ML}}\frac{\partial \psi_{\mathrm{ML}}}{\partial t} = -F_{\psi,T} + F_{\psi,0} - \Delta F. \tag{5.38}$$

Assuming that ψ_{cld} and ψ_{sub} do not change, but z_{cb} and z_{ML} do change, ψ_{tr} should change according to:

$$\begin{aligned} & z_{\mathrm{cld}}\psi_{\mathrm{cld}} + \left(z_{\mathrm{cb}} - z_{\mathrm{ML}}\right)\psi_{\mathrm{tr}} + z_{\mathrm{ML}}\psi_{\mathrm{ML}} = \\ & \left(z_{\mathrm{cld}} + dz_{\mathrm{cld}}\right)\psi_{\mathrm{cld}} + \left(z_{\mathrm{cb}} + dz_{\mathrm{cb}} - z_{\mathrm{ML}} - dz_{\mathrm{ML}}\right)\left(\psi_{\mathrm{tr}} + d\psi_{\mathrm{tr}}\right) + \left(z_{\mathrm{ML}} + dz_{\mathrm{ML}}\right)\psi_{\mathrm{ML}}. \end{aligned} \tag{5.39}$$

6 Set-up of the experiments

In this section the set-up of the experiments as well as the motivation to do these experiments is explained. The constants that are used for the experiments are displayed in table 6.1.

6.1 Transient solutions

The transient solutions are obtained as described in section 5.2. For the critical relative humidity $\mathrm{RH}_{\mathrm{crit}} = 0.99$ has been chosen.

6.1.1 Validation of the two-layer model

The two-layer model should accurately predict the development of the boundary layer over a period of time and should also be able to predict stratocumulus to cumulus transition as most of the uncertainties in cloud-climate feedback arise from the stratocumulus and stratocumulus to cumulus transition regimes [Williams and Webb, 2009].
To test the results from the two-layer model, the Atlantic Stratocumulus Transition EXperiment (ASTEX) is used as a reference. This field experiment was conducted in 1992 over the northeast Atlantic Ocean. In this experiment air traveling over sea was followed to study the stratocumulus to cumulus transition for a period of 40 hours. The initial profiles are taken from this case, as well as the time-varying boundary conditions such as the sea surface temperature and the large-scale divergence of horizontal winds.
Sandu and Stevens showed in an LES study that LES models can represent these cloud transition cases very well. The LES results obtained with DALES by Johan van der Dussen are therefor used to compare the results.
The radiative cooling has been set to the average net radiative cooling of ASTEX: $\Delta F_{\mathrm{rad}} = 43$ W/m^2. All constants used from ASTEX are displayed in table 6.2.

Table 6.1 – Input parameters for the experiments.

Input parameter	Value	Input parameter	Value
L_v	$2.5008 \cdot 10^6$ J	c_p	1004 J/(kg $\cdot$ K)
U	10 m/s	g	9.80665 m/(s^2)
R_{d}	287.06 J/(kg $\cdot$ K)	p_0	$1 \cdot 10^5$ Pa
R_{v}	461.5 J/(kg $\cdot$ K)	ρ	1.1436 kg/m^2
C_d	0.001		

Table 6.2 – Input parameters for the transient experiments.

Input parameter	Value
p_{sfc}	102900 Pa
ΔF_{rad}	43 W/m^2
$\Gamma_{q_{\mathrm{t}}}$	$-2.8 \cdot 10^{-6}$ m^{-1}
Γ_θ	$5.5 \cdot 10^{-3}$ K/m

6.1.2 Subsidence experiment

A subsidence experiment is set up to determine the sensitivity of the development of the boundary layer, and in particular the LWP, to differences in subsidence. The motivation for this experiment is the uncertainty in the subsidence rate during the ASTEX transition [Bretherton and Pincus, 1995]. Bretherton and Pincus stated the hypothesis that the decreasing subsidence observed in ASTEX led to the break-up of the cloud layer.
However, in more recent research it is found that the decrease of subsidence actually leads to deepening of the cloud [de Roode and van der Dussen, 2010, Sandu and Stevens, 2011, van der Dussen, 2012, Bretherton et al., 2013].
The subsidence experiment in this thesis is conducted with three different divergences as a function of time, similar to the research done by van der Dussen [2012]. The different divergences used are introduced in section 7.3 and displayed in figure 7.7.

6.2 Steady-state solutions

This part of the research focuses on the steady-state solutions. The equilibrium solutions can only be physically representative if the adjustment time-scale of the boundary layer is much shorter than the time scale over which the forcings change [Zhang, 2009]. These steady state solutions are therefore very useful to research the feedback to climate changes. In this thesis these solutions will be used to study the feedback of clouds to an increase in SST. The steady-state solutions are obtained according to the method described in section 5.1.
To obtain the steady state solutions in a decoupled system, a decoupling parameter r_ψ must be used. Wood and Bretherton [2004] did an observational study to marine boundary layer depth and the degree of decoupling in different regions of the tropical and subtropical east Pacific. From these observations the median values of α_θ and α_q have been found and are shown in table 6.3. The magnitude of the decoupling parameters can be estimated using the data of Wood and Bretherton from table 6.3 and the simplified relation:

$$\alpha_\psi \approx r_\psi z_i, \tag{6.1}$$

Table 6.3 – Median values of α_θ and α_q for five different regions [Wood and Bretherton, 2004].

Region	Longitude	Latitude	α_θ	α_q	$\overline{z_i}$ [m]
a	$120° - 130°$W	$25° - 35°$N	0.15 ± 0.08	0.18 ± 0.06	1200 ± 100
b	$135° - 150°$W	$15° - 25°$N	0.30 ± 0.10	0.32 ± 0.08	1730 ± 250
c	$80° - 90°$W	$15° - 25°$S	0.11 ± 0.07	0.13 ± 0.06	1140 ± 100
d	$100° - 110°$W	$5° - 15°$S	0.24 ± 0.08	0.27 ± 0.08	1560 ± 200
e	$90° - 110°$W	$5°$S $- 5°$N	0.29 ± 0.08	0.33 ± 0.07	1535 ± 200

that was introduced in equation (5.21) to allow for an analytical solution. Using this relation and the measurements of table 6.3, r_ψ is estimated in table 6.5. Based on these values $r_q = 1.7 \cdot 10^{-4}$ and $r_\theta = 0.89 r_q$ have been chosen.
Other parameters used for the steady-state experiments are given in table 6.4.

6.2.1 Validation of the entrainment parameterisation

Since the Nicholls-Turton entrainment parameterisation is difficult to apply in a two-layer system, as explained in 4.1, the entrainment parameterisation of equation 4.12 is used. To test if it is valid to use this parameterisation, results from the two-layer model without decoupling are compared with results from de Roode et al., who used the Nicholls-Turton parameterisation.

6.2.2 Steady-state experiments with the two-layer model

In the experiments of de Roode et al. the steady-state solutions of the boundary layer are obtained for different free tropospheric conditions. The ranges considered are $18 < \mathrm{LTS} < 30$ K and $0 < q_{\mathrm{t,ft}} < 10$ g/kg, which avoid condensation in the free troposphere.
The same experiments are done with the two-layer model to observe the effect of decoupling in the steady state of the boundary layer. The effect on the LWP is especially interesting, as the MLM tends to overestimate the LWP [Caldwell et al., 2012].

Table 6.4 – Input parameters for the steady-state experiments.

Input parameter	Value	Input parameter	Value
D	$5 \cdot 10^{-6}$ s^{-1}	ΔF_{rad}	40 W/m^2
SST	289.5 K	θ_{ref}	286 K
p_{sfc}	101900 Pa	Γ_θ	$6 \cdot 10^{-3}$ K/m

Table 6.5 – Deduced decoupling parameters r_θ and r_q from equation 6.1 and table 6.3.

Region	r_θ	r_q	$\frac{r_\theta}{r_q}$
a	$1.3 \cdot 10^{-4} \pm 5.8 \cdot 10^{-6}$	$1.5 \cdot 10^{-4} \pm 4.2 \cdot 10^{-6}$	$0.87 \pm 4,6 \cdot 10^{-2}$
b	$1.7 \cdot 10^{-4} \pm 8.2 \cdot 10^{-6}$	$1.8 \cdot 10^{-4} \pm 6.5 \cdot 10^{-6}$	$0.94 \pm 5.7 \cdot 10^{-2}$
c	$9.6 \cdot 10^{-5} \pm 5.4 \cdot 10^{-6}$	$1.1 \cdot 10^{-4} \pm 4.5 \cdot 10^{-6}$	$0.87 \pm 6.1 \cdot 10^{-2}$
d	$1.5 \cdot 10^{-4} \pm 6.4 \cdot 10^{-6}$	$1.7 \cdot 10^{-4} \pm 6.5 \cdot 10^{-6}$	$0.88 \pm 5.1 \cdot 10^{-2}$
e	$1.9 \cdot 10^{-4} \pm 6.8 \cdot 10^{-6}$	$2.1 \cdot 10^{-4} \pm 5.8 \cdot 10^{-6}$	$0.90 \pm 4.1 \cdot 10^{-2}$

6.2.3 Response LWP to perturbed SST

To discover the change in radiative effect of stratocumulus clouds in a warming climate, a steady state experiment is done in which the SST is perturbed by 1 K, similar to the experiment from de Roode et al. [2012]. Since the liquid water path (LWP) determines to the first order the albedo, the response of the LWP to a perturbed SST is examined.

7 Transient solutions with the two-layer model

The transient solutions are obtained according to the method described in section 5.2 and in the set-up described in section 6.1.

7.1 Time evolution and comparison with LES results

In figures 7.1 and 7.2 the time evolutions based on the input from ASTEX can be seen for the two-layer model with decoupling parameters $r_q = 9 \cdot 10^{-4}$ and $r_\theta = 0.4 r_q$ and for the case where there is no decoupling. Also the LES results obtained with DALES by van der Dussen et al. [2013] of the ASTEX case are plotted in the same figures to compare the model results with the LES results as explained in section 6.1. The vertical profiles of these results can be found in figure 7.3. The cloud and sub-cloud values of θ_l and q_t have been estimated from the LES results.

In all model results the inversion layer height z_i grows in time. As an explanation, the entrainment causes a growth of z_i, while the subsidence $\overline{w}$ pushes it down, but since $w_\mathrm{e} > \| \overline{w} \|$ there is a rapid growth in z_i. Both the MLM and the two-layer model overestimate z_i in the first 20 hours and after that underestimate z_i.

Due to a positive surface heat flux and the mixing of warm and dry air at the top of the cloud, the boundary layer warms. It can therefore be seen that $\theta_\mathrm{l,ML}$ and $\theta_\mathrm{l,cld}$ both increase with time. From the LES and the two-layer model results it can be seen that $\theta_\mathrm{l,cld}$ grows faster than $\theta_\mathrm{l,ML}$. This is because the growing inversion layer height increases the amount of decoupling by equation (5.5). The increasing amount of decoupling pushes the cloud and sub-cloud layer further apart, causing the cloud layer to warm even more. In the case where ther is no decoupling, $\theta_\mathrm{l,ML}$ and $\theta_\mathrm{l,cld}$ are the same.

A positive surface humidity flux results in a moister sub-cloud layer as can be observed from the growth of $q_\mathrm{t,ML}$. For the MLM the turbulent eddies are able to transport the moisture throughout the mixed layer. For the MLM $q_\mathrm{t,ML} = q_\mathrm{t,cld}$ and therefore also $q_\mathrm{t,cld}$ grows in time. In the two-layer model the decoupling requires the cloud layer to be dryer than the sub-cloud layer. Dry and warm air is mixed into the cloud layer causing the drying of the cloud layer, which can be seen in the results of the two-layer model and the LES model. Even in a qualitative comparison of $q_\mathrm{t,cld}$ the MLM predictions are not correct, while the two-layer model gives similar results as the LES model.

The warming of the boundary layer leads to an increase in both z_cb and z_ML. Because of the drying of the cloud layer in the two-layer model, z_cb becomes much higher there than in the MLM. For both z_ML and z_cb the two-layer model results are much closer to the LES results than the MLM results.

The predictions of the cloud thickness and LWP are much closer to the LES results when using the two-layer model instead of the MLM. The MLM predicts an increasing LWP in time, while the LES results show a decreasing LWP. The two-layer model is able to capture the same development as the LES model and also shows a decreasing LWP.

7.2 Effect of the decoupling rate on boundary layer evolution

In figures 7.4 and 7.5 time evolutions for different decoupling parameters are displayed. In figure 7.6 the vertical profiles of the same evolution are displayed at hours 20, 30 and 40.
For a larger decoupling, z_i grows faster. The entrainment rate obeys the decoupling equation (5.4) and therefore increases for a larger decoupling to warm and dry the cloud layer. As the entrainment rate determines the growth of the inversion layer, z_i grows faster for a larger decoupling.
From $\theta_{\mathrm{l,cld}}$ and $q_{\mathrm{t,cld}}$, it can also be seen that for a larger rate of decoupling the cloud layer becomes dryer and warmer, as expected. The saturation point is therefore found at a higher level, explaining the increased z_{cb}.
Both z_i and z_{cb} increase for all decoupling parameter values, but for a larger decoupling z_{cb} grows faster than z_i. More decoupling therefore leads to smaller cloud thickness and a smaller LWP.

7.3 Effect of subsidence on the boundary layer evolution

To examine the influence of the subsidence on the transient solutions, three different large-scale divergences of horizontal winds have been used, as shown in figure 7.7. In figures 7.8 and 7.9 the time dependent solutions can be observed for the different divergences. In figure 7.10 the vertical profiles of θ_l and q_t for hours 20, 30 and 40 are displayed.
The results show a faster growing z_i for smaller divergence. As an explanation, the entrainment causes the BL to grow, while the subsidence pushes it down. A smaller divergence leads to a smaller subsidence which results in a faster growing z_i.
A smaller divergence leads to a higher boundary layer, but also to more decoupling according to equation (5.5). The entrainment rate should obey the decoupling principle by the design of the two-layer model from section 5.2 and will increase to create a warming and drying of the cloud layer.
A different divergence has no influence on $\theta_{\mathrm{l,ML}}$ since its tendency depends on the surface flux according to equation 5.26 which is not influenced by the different divergence.
As a smaller divergence leads to a higher boundary layer, it also results in a larger

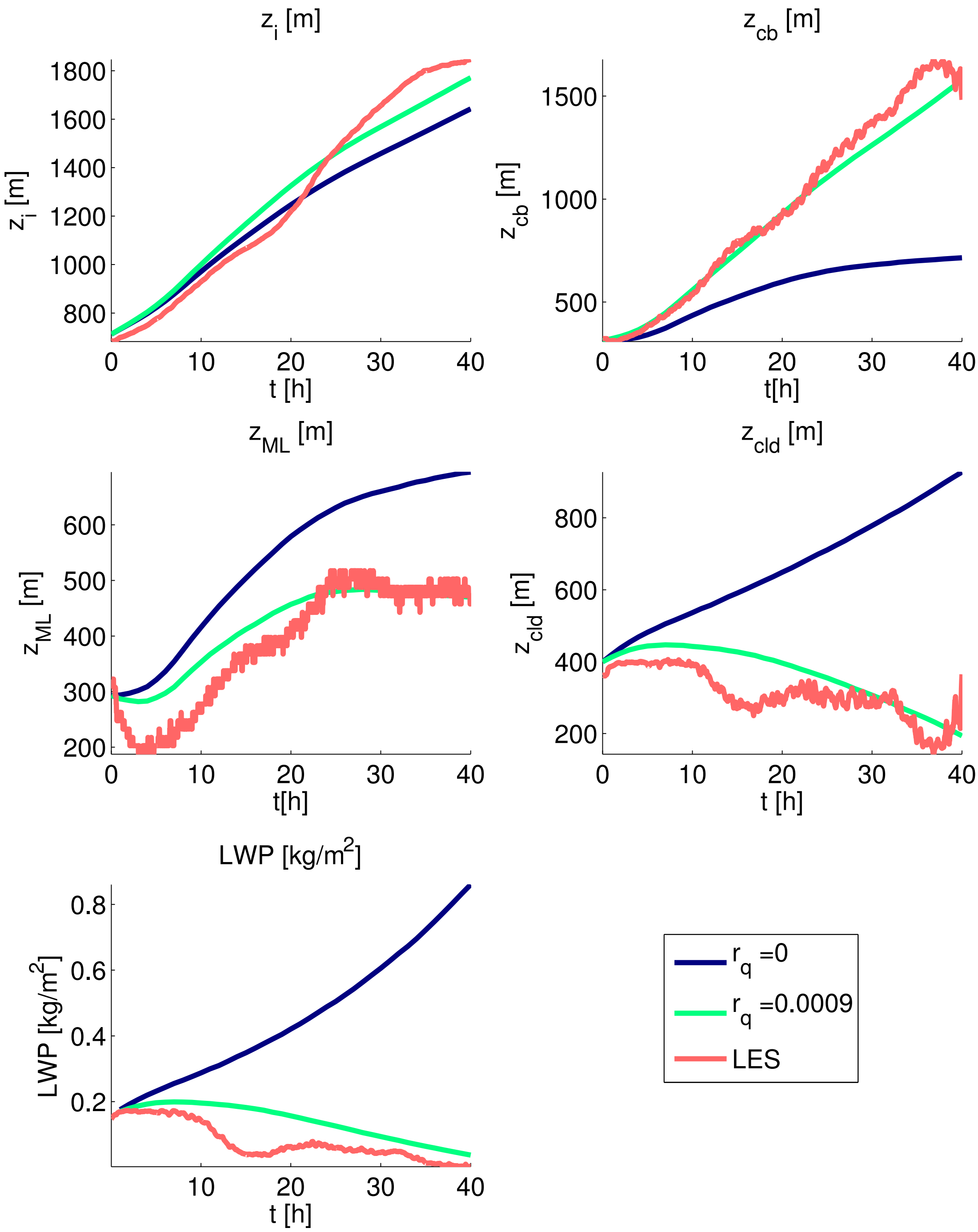

Figure 7.1 – Time evolution of z_i, z_cb, z_ML, z_cld and the LWP of the LES results and of the two-layer model with decoupling parameters $r_q = 9 \cdot 10^{-4}$ and $r_\theta = 0.4 r_q$ and RH$_\mathrm{crit}= 0.99$.

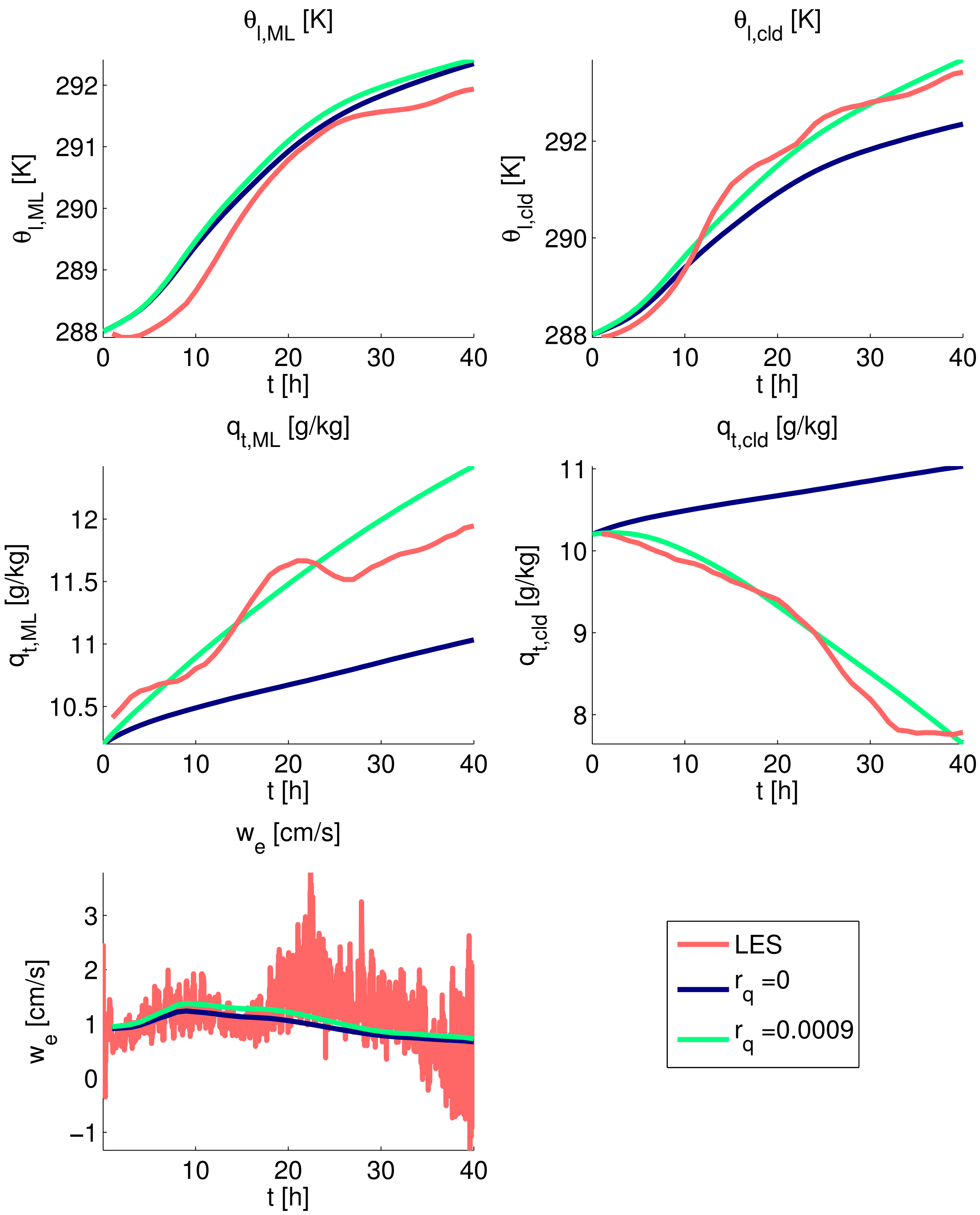

Figure 7.2 – Time evolution of $\theta_{\mathrm{l,ML}}$, $\theta_{\mathrm{l,cld}}$, $q_{\mathrm{t,ML}}$, $q_{\mathrm{t,cld}}$ and w_{e} of the LES results and the two-layer model with decoupling parameters $r_q = 9 \cdot 10^{-4}$ and $r_\theta = 0.4 r_q$ and RH$_{\mathrm{crit}} = 0.99$.

decoupling according to equation (5.5). This larger decoupling results in a sub-cloud layer that is more moist. From equation (5.16) it could be seen that for larger decoupling the humidity state of the sub-cloud layer is pushed towards the surface humidity.
The increased entrainment rate for smaller subsidence leads to a dryer and warmer cloud, as warm and dry air from above the inversion is mixed into the cloud layer. Due to this warmer and dryer cloud layer, the cloud base height will also increase. For a smaller divergence both z_{i} and z_{cb} will get higher, but z_{i} grows more than z_{cb} leading to a thicker cloud. For smaller divergences the cloud thickness and therefore the LWP will be larger. This is accordance with earlier results by de Roode and van der Dussen [2010], Sandu and Stevens [2011], van der Dussen [2012], Bretherton et al. [2013].

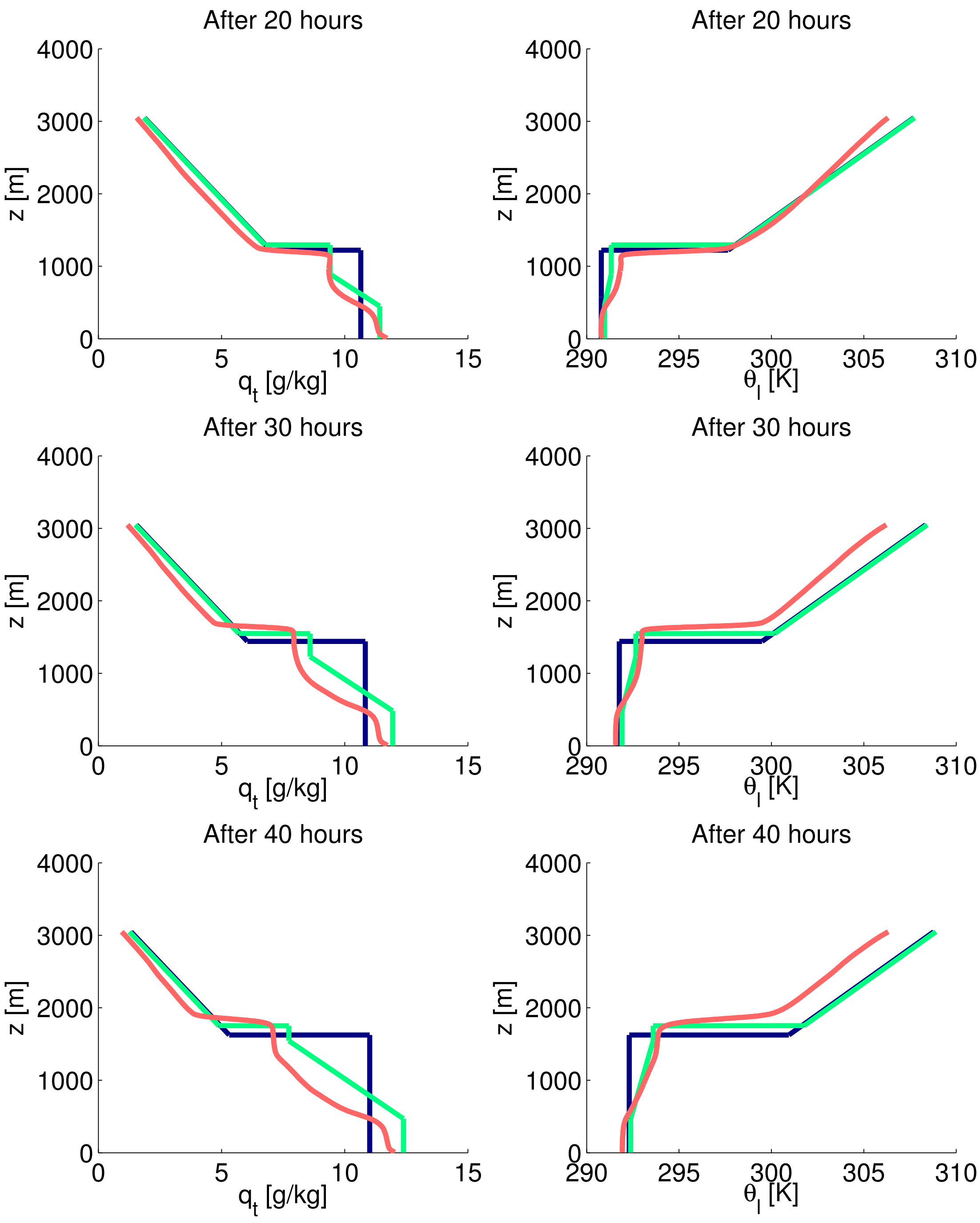

Figure 7.3 – The vertical profiles of q_{t} and θ_{l} plotted for hours 20, 30 and 40 for decoupling parameters $r_q = 9 \cdot 10^{-4}$ and $r_\theta = 0.4 r_q$ and RH$_{\mathrm{crit}}$= 0.99. The line styles are the same as in figures 7.1 and 7.2.

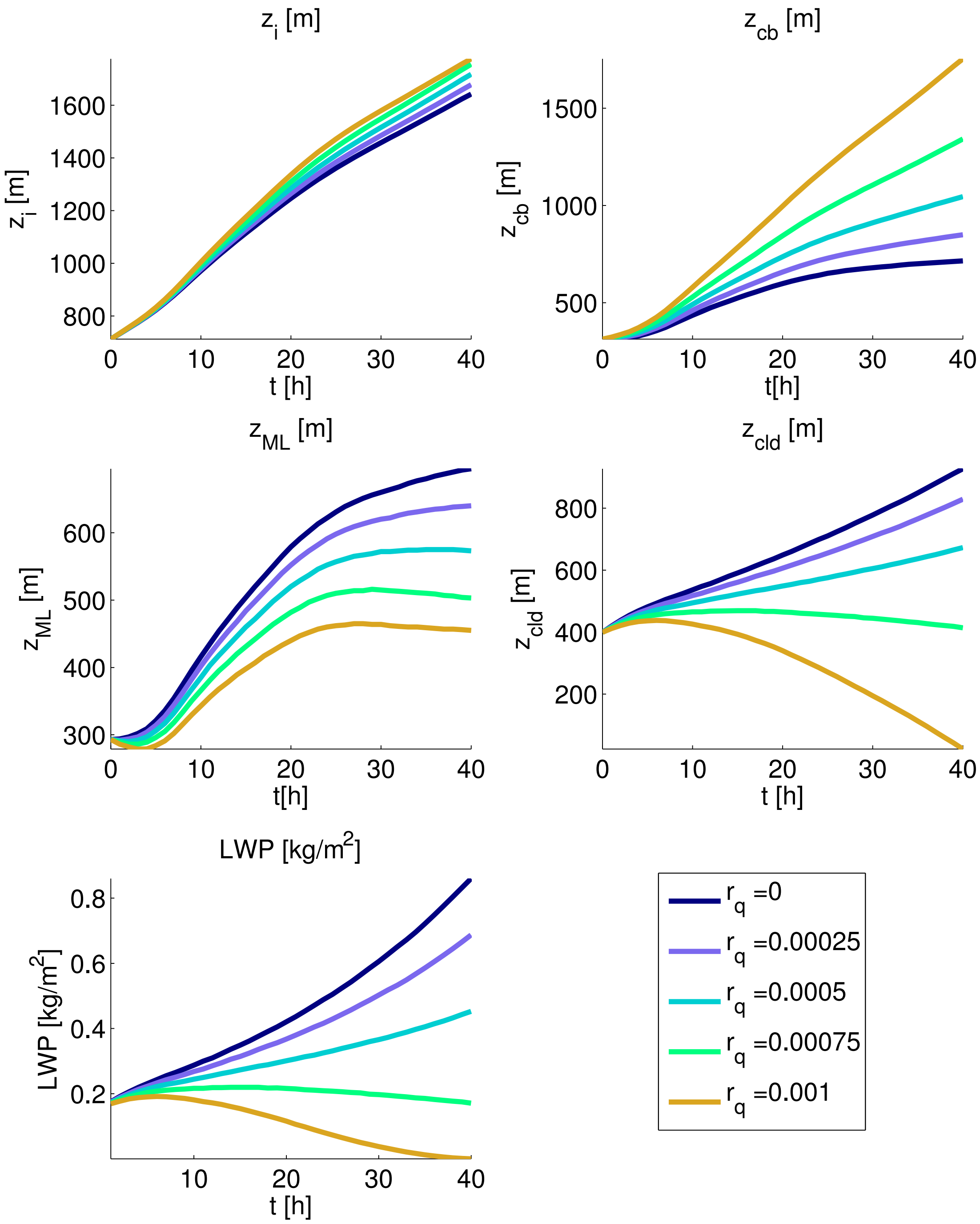

Figure 7.4 – Evolution of z_{i}, z_{cb}, z_{ML}, z_{cld} and LWP for different decoupling parameters where $r_\theta = 0.4 r_q$ and RH$_{\mathrm{crit}} = 0.99$.

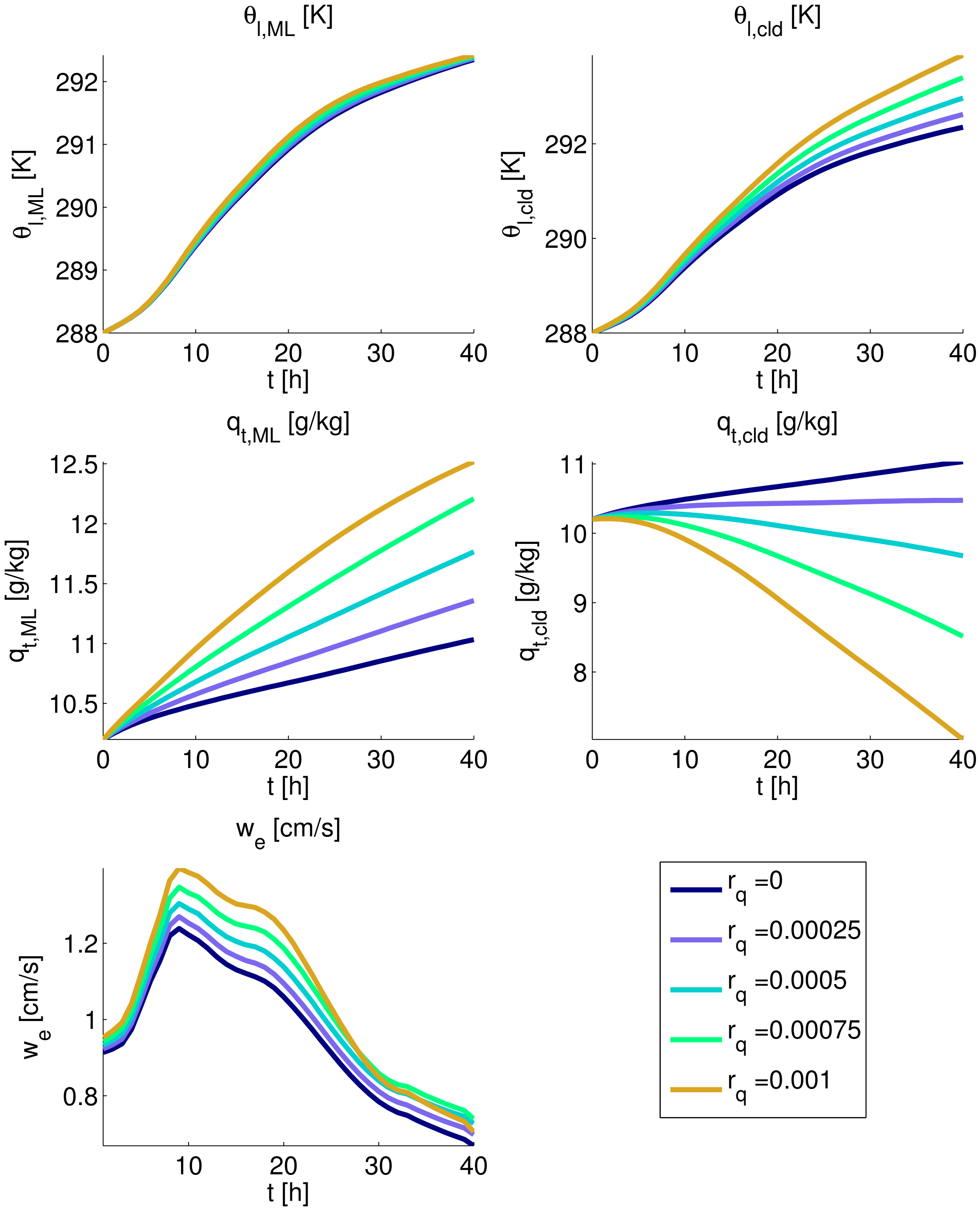

Figure 7.5 – Evolution of $\theta_{\mathrm{l,ML}}$, $\theta_{\mathrm{l,cld}}$, $q_{\mathrm{t,ML}}$, $q_{\mathrm{t,cld}}$ and w_{e} for different decoupling parameters where $r_\theta = 0.4 r_q$ and RH$_{\mathrm{crit}}$$= 0.99$.

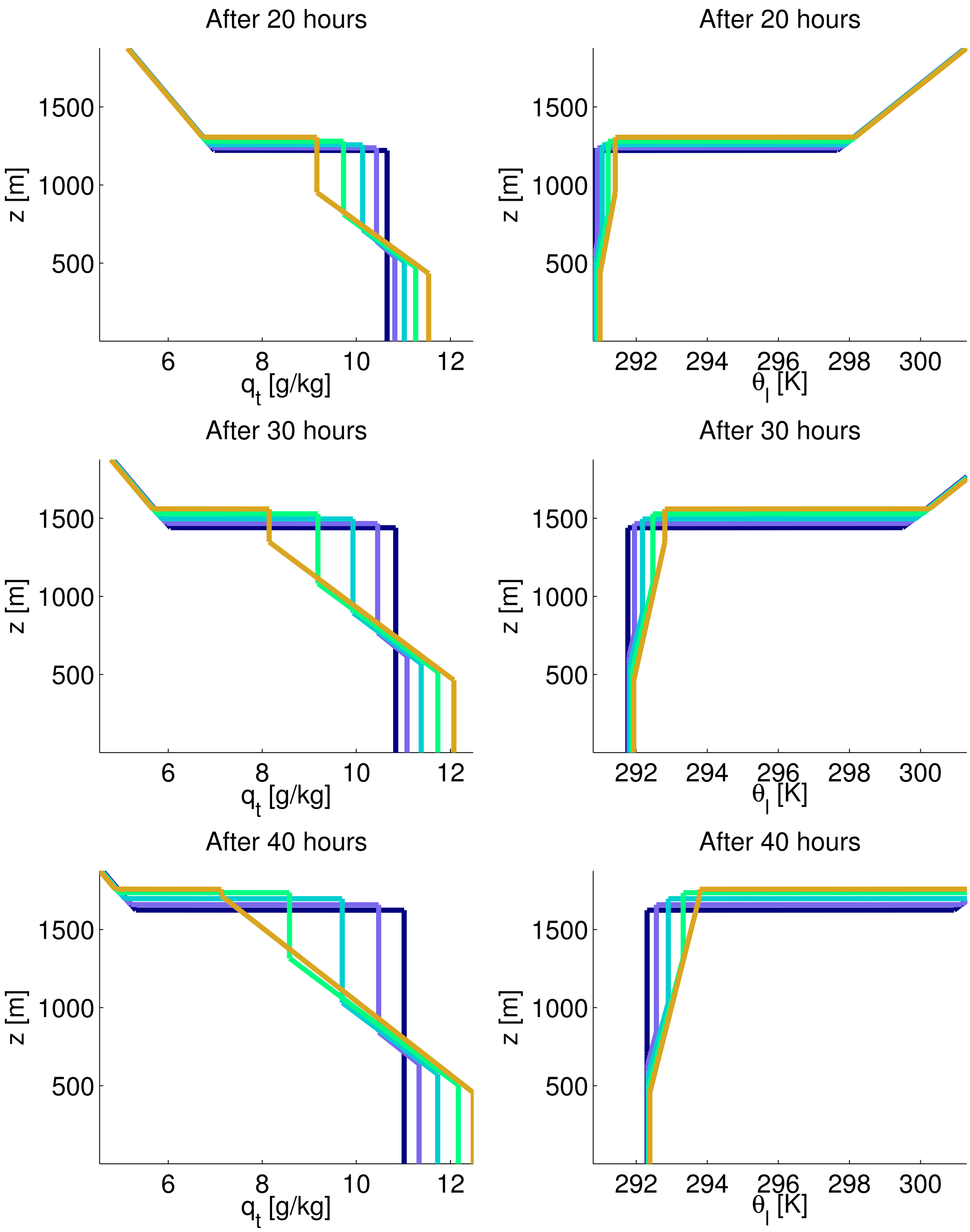

Figure 7.6 – Vertical profiles of θ_l and q_t for hours 20, 30 and 40 for different decoupling parameters. The line styles are the same as in figures 7.4 and 7.5.

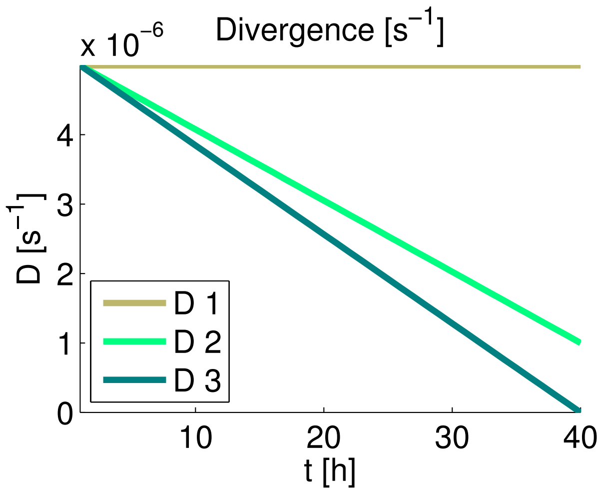

Figure 7.7 – Different divergences used, varying in time. The second divergence is the same as prescribed in the ASTEX case.

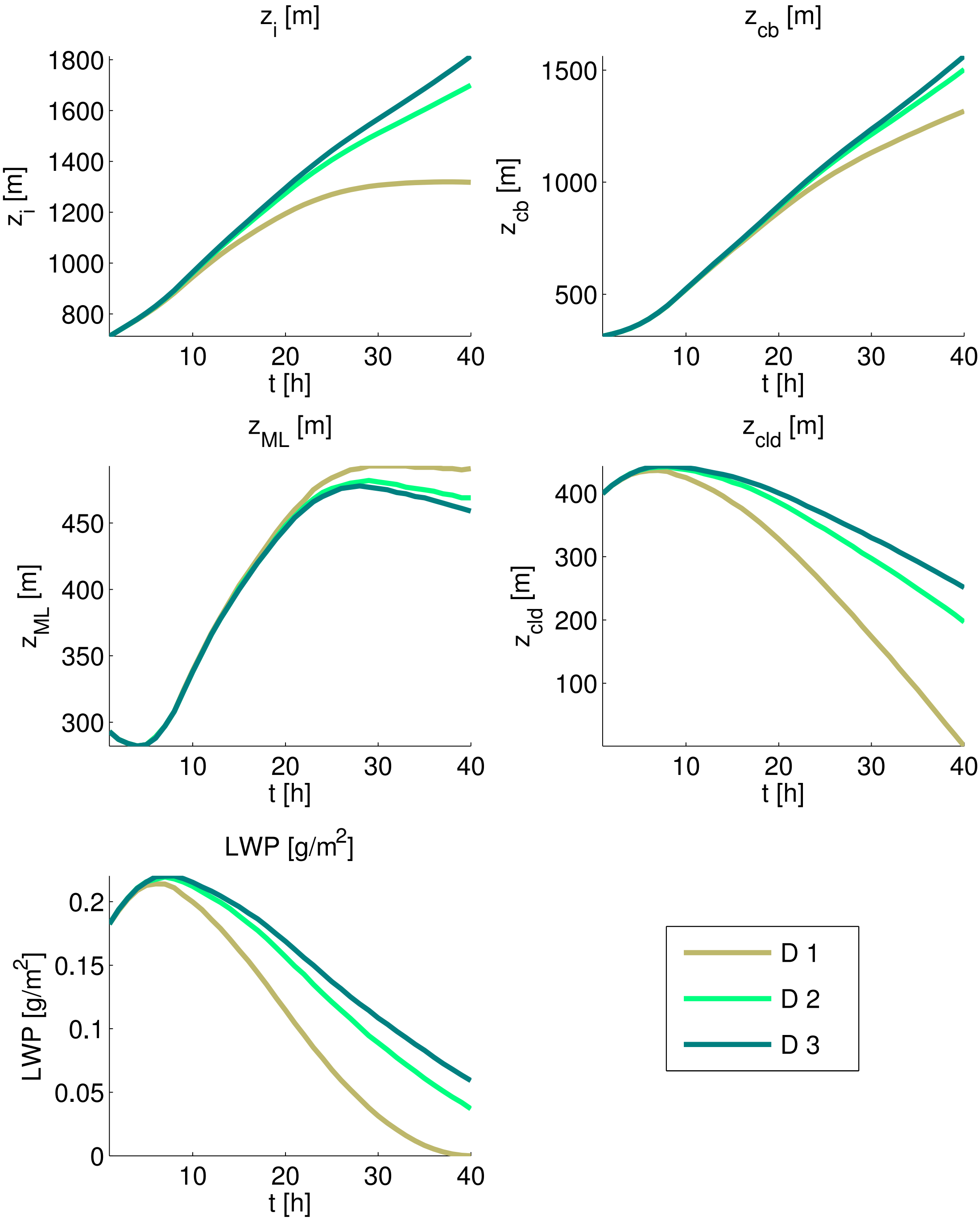

Figure 7.8 – Time-dependent solutions of z_i, z_cb, z_ML, z_cld and LWP for different divergences with $r_q = 9 \cdot 10^{-4}$ and $r_\theta = 0.4 r_q$.

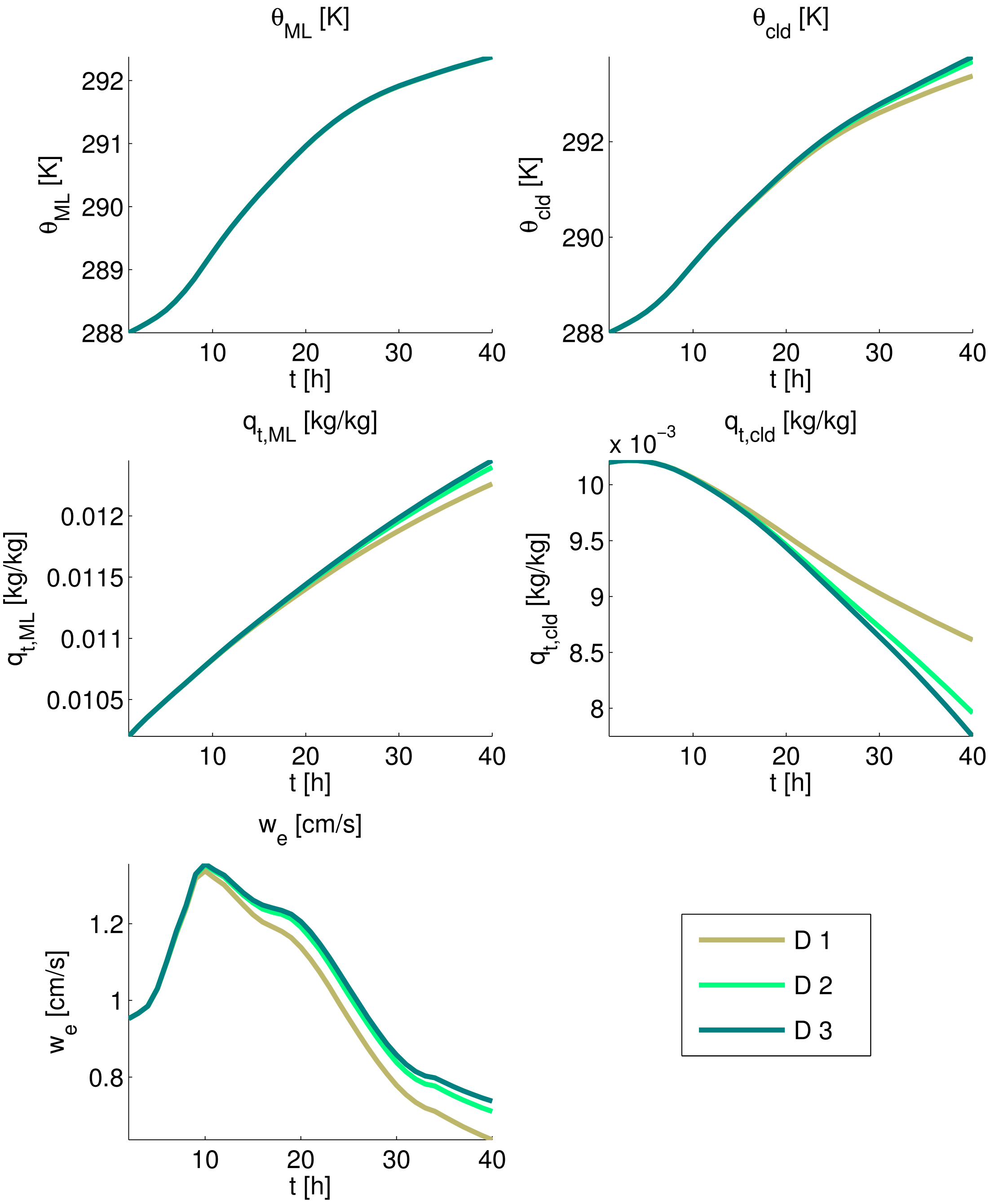

Figure 7.9 – Time-dependent solutions of $\theta_{\mathrm{l,ML}}$, $\theta_{\mathrm{l,cld}}$, $q_{\mathrm{t,ML}}$, $q_{\mathrm{t,cld}}$ and w_{e} for different divergences with $r_q = 9 \cdot 10^{-4}$ and $r_\theta = 0.4 r_q$.

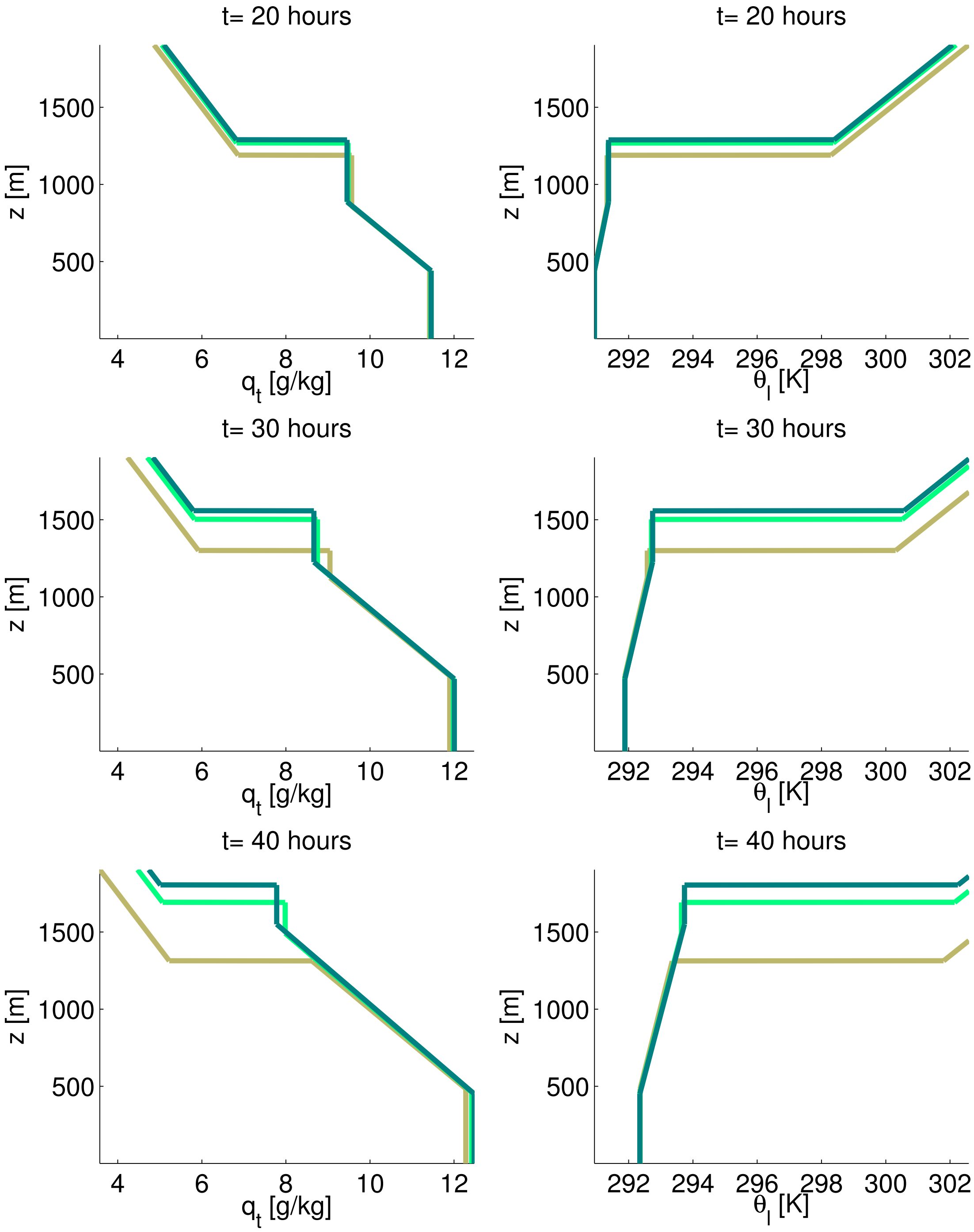

Figure 7.10 – Vertical profiles of θ_l and q_t for three different divergences with $r_q = 9 \cdot 10^{-4}$ and $r_\theta = 0.4 r_q$. The linestyles are the same as in figures 7.8 and 7.9.

8 Steady-state solutions

The steady-state solutions are obtained with the method described in section 5.1 and the set-up of the experiments is described in section 6.2.

8.1 Validation of the entrainment parameterisation

In figure 8.1 the steady-state solutions for the boundary layer for a range of free tropospheric conditions are showed, that are obtained by de Roode et al. [2012]. These are used as a reference to validate the use of the entrainment parameterisation given in equation (4.12).
In figure 8.2 the steady-state solutions in the same phase-space as the results from de Roode et al. are displayed. The efficiency factor used is $\eta = 0.8$. There are differences between the results obtained with different entrainment parameterisations. Due to a constant efficiency factor the free tropospheric humidity does not have any effect on the inversion layer height, while $q_{\mathrm{t,ft}}$ has an effect when using the Nicholls-Turton parameterisation. The same curvature as in the plots of de Roode et al. is therefore not found.
Apart from this small difference, the results obtained with the simple entrainment parameterisation are similar to those using a more advanced entrainment parameterisation such as the Nicholls-Turton parameterisation. Apparently the simple form used here is able to capture a similar behaviour.

To quantitatively approach the results of De Roode et al. as much as possible, different entrainment efficiencies have been used. In figure 8.3 and 8.4 the results for $\eta = 1.0$ and $\eta = 0.6$ are shown respectively. The efficiency factor of $\eta = 0.7$, used by Dal Gesso et al., gives results similar to figure 8.1 for higher LTS, while the high efficiency factor $\eta = 1.0$ gives results more similar for lower LTS.
After comparing more results with different efficiency factors, $\eta = 0.8$ is chosen to be an appropriate constant when using a constant η, since the results obtained then are close to the results obtained with the Nicholls-Turton entrainment parameterisation.

8.2 Results with the two-layer model

The steady-state solutions of the boundary layer for a range of free tropospheric conditions are also obtained with the two-layer model to visualize the effect of the decoupling. The decoupling parameters used are $r_q = 1.7 \cdot 10^{-4}$ and $r_\theta = 0.89 r_q$ as explained in section 6.2. In figure 8.5 the steady state solutions with these decoupling parameters can be seen. When comparing these plots to the results of the MLM from figure 8.2, several differences are observed.
In the decoupled system $\theta_{\mathrm{l,cld}}$ is higher and $q_{\mathrm{t,cld}}$ lower, according to the design of

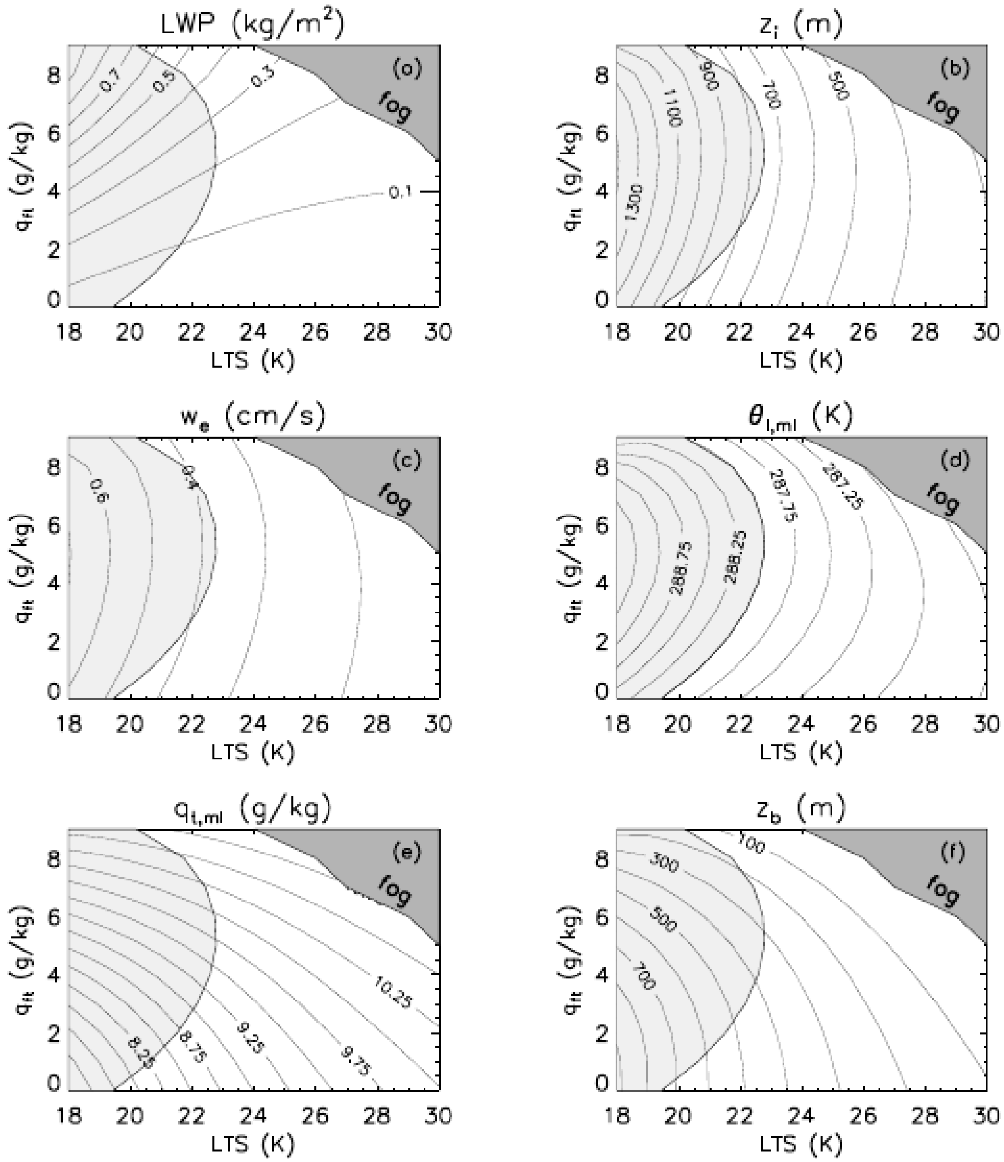

Figure 8.1 – Steady-state solutions of the mixed layer model as a function of the LTS and $q_{\mathrm{t,ft}}$ with Nicholls-Turton entrainment parameterisation. Figure copied from de Roode et al. [2012].

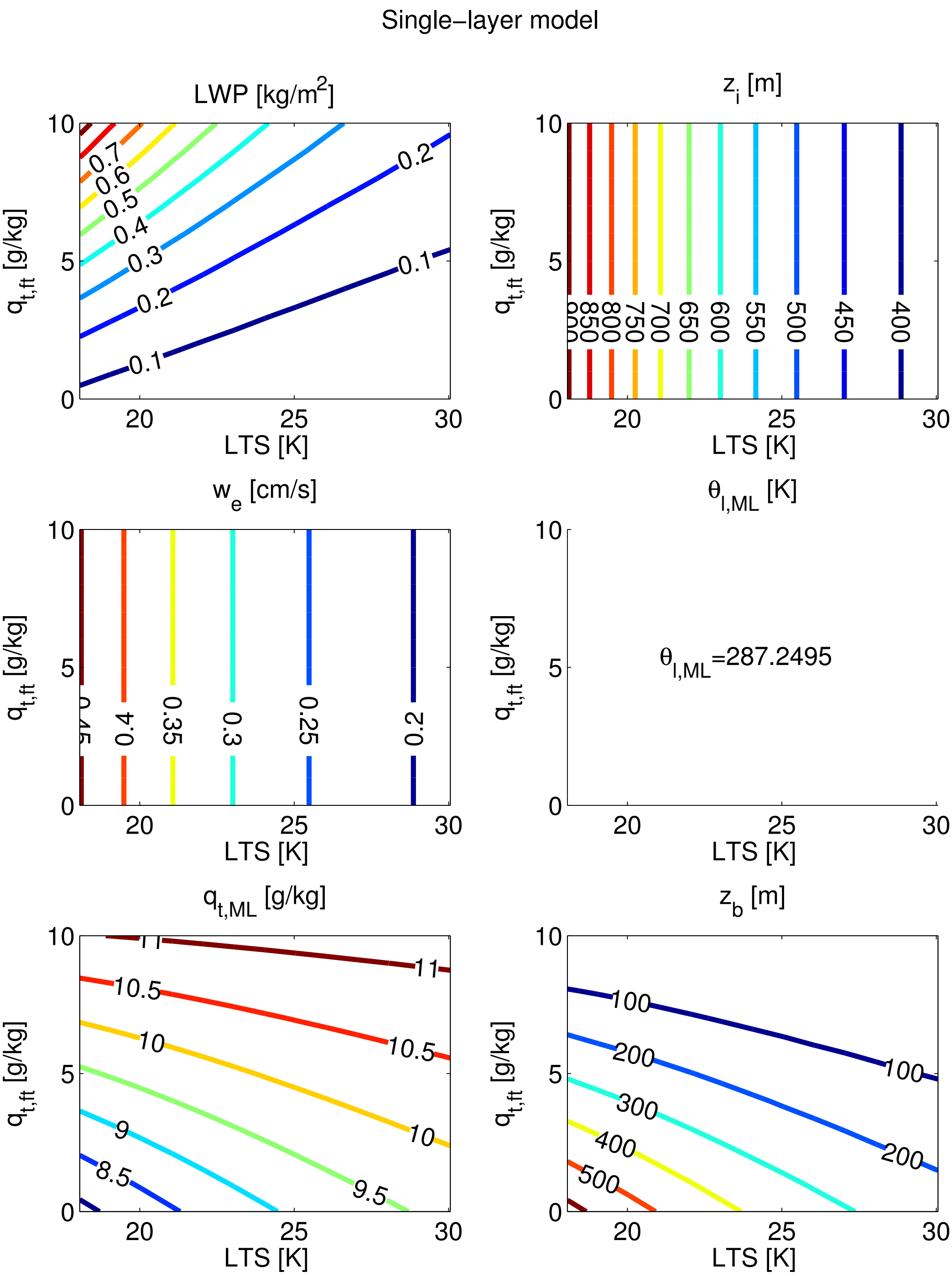

Figure 8.2 – Steady-state solutions of the single-layer model as a function of the LTS and $q_{\mathrm{t,ft}}$, $\eta = 0.8$.

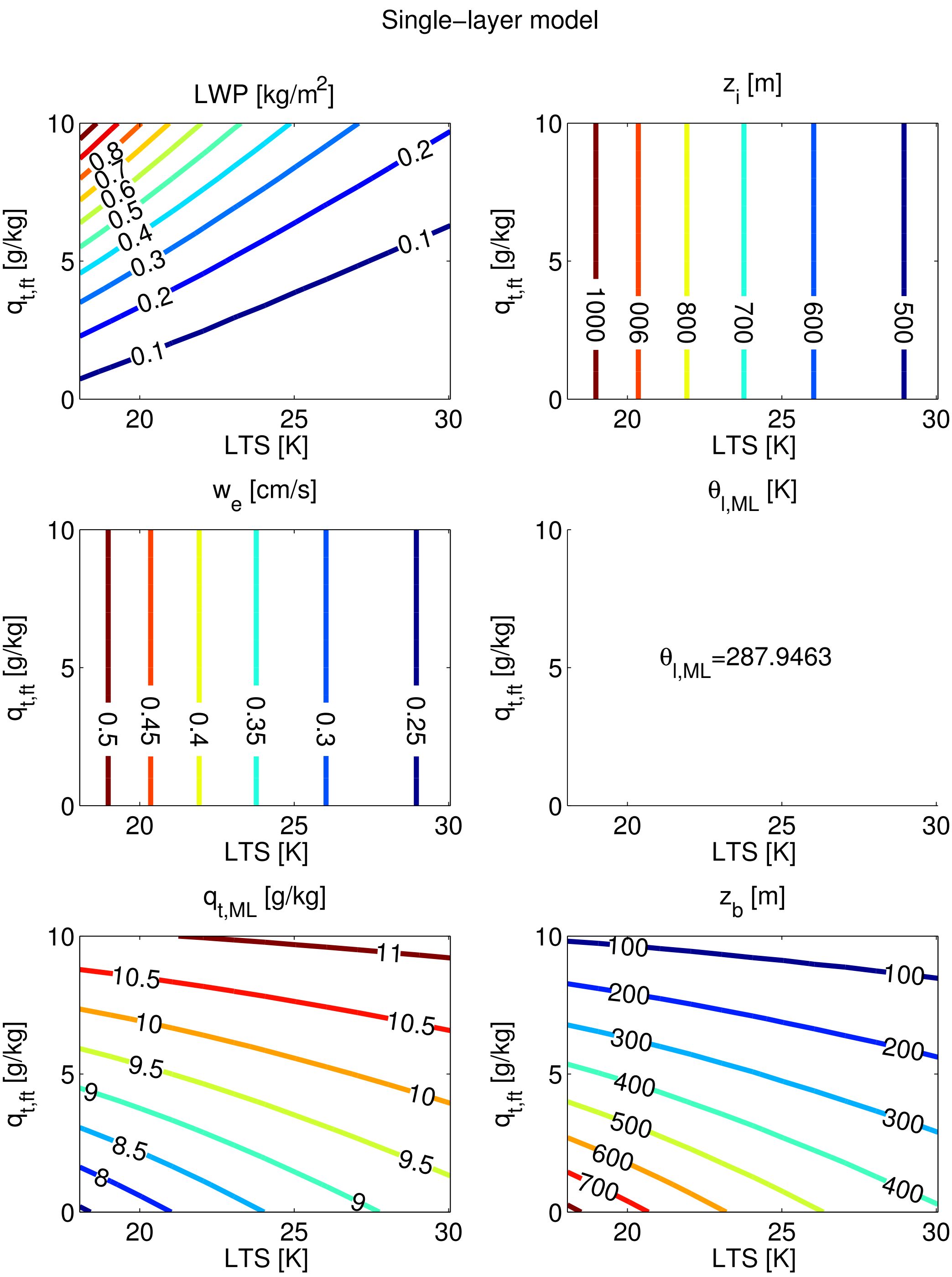

Figure 8.3 – Steady-state solutions of the single-layer model as a function of the LTS and $q_{\mathrm{t,ft}}$, $\eta = 1.0$.

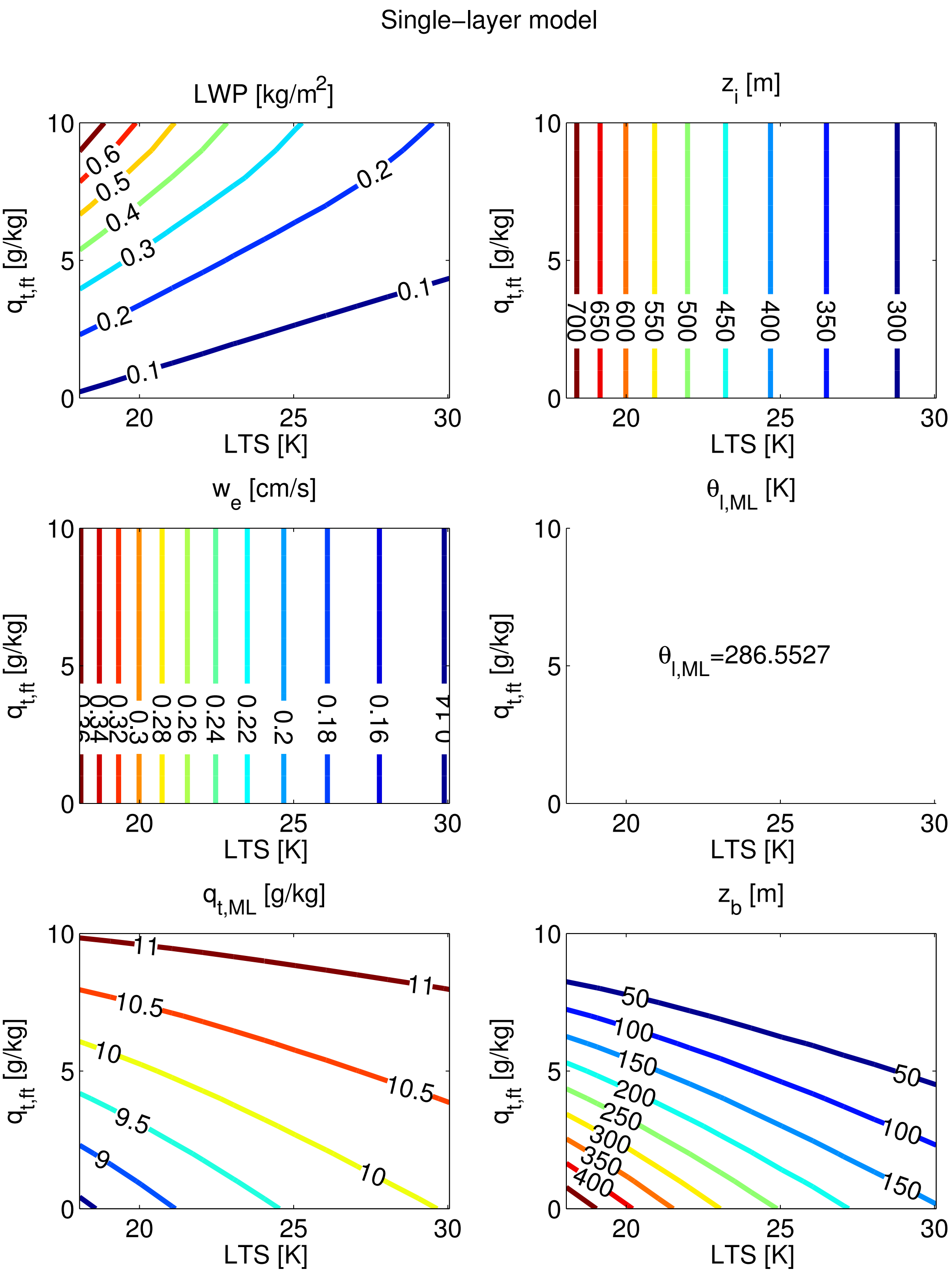

Figure 8.4 – Steady-state solutions of the single-layer model as a function of the LTS and $q_{t,ft}$, $\eta = 0.6$.

the two-layer model. The warmer and dryer cloud results in a higher cloud base hight.
Due to the warmer and dryer cloud the temperature jump over the inversion layer has decreased, as can be seen from the higher entrainment rate w_e. This entrainment leads to an increase in inversion layer height z_i.
Despite the fact that z_i is higher than in the single-layer model, the LWP is smaller in the decoupled system, since z_cb increases more than z_i. As mentioned before, the MLM overpredicts the LWP [Caldwell et al., 2012]. This smaller LWP is more realistic when comparing these results to observations and LES results.

8.2.1 Response LWP to perturbed SST

The effect of warming of the sea surface to the LWP is simulated by raising the SST as explained in section 6.2.3. In figure 8.6 the total response of the LWP can be seen for the MLM.
The LWP increases over the whole domain when raising the SST, indicating a cloud thickening for all free tropospheric conditions.
In figure 8.7 the total change of the LWP for perturbed SST is plotted for the two-layer model with decoupling parameters $r_q = 1.7 \cdot 10^{-4}$ and $r_\theta = 0.89 r_q$, where the entrainment rate was allowed to respond to the change in SST.
Three areas can be distinguished. For very low values of $q_\mathrm{t,ft}$, the response of the LWP is zero, indicated by the white area in the figure. This is because the LWP for this rate of decoupling is zero as can be seen from figure 8.5. The raise of SST does not change the absence of clouds and therefore the response of LWP to the raise in SST is zero.
For the lower part of the LTS values, a green area indicates the positive response of the LWP. The response to a sea surface warming is a cloud thickening, but the thickening is smaller than predicted by the MLM.
For the higher part of the LTS values, an orange area indicates the negatice response of the LWP. The two-layer model predicts a cloud thinning for these free tropospheric conditions, while the MLM predicts a cloud thickening for all free tropospheric conditions.
In figure 8.8 the response of the LWP to the change in SST is displayed for different decoupling parameters.
For small decoupling such as $r_q = 1 \cdot 10^{-4}$ the response of the LWP is positive for most free tropospheric conditions. For large values of the LTS (LTS $>$ 26 K) the response is negative.
Higher decoupling parameters ($r_q \geq 2 \cdot 10^{-4}$) result in a larger part where the response of the LWP is zero. In these areas the steady-state solutions predict an LWP of zero. Changing the SST does not result in the formation of clouds and therefore the response of the LWP is also zero. Larger decoupling results in

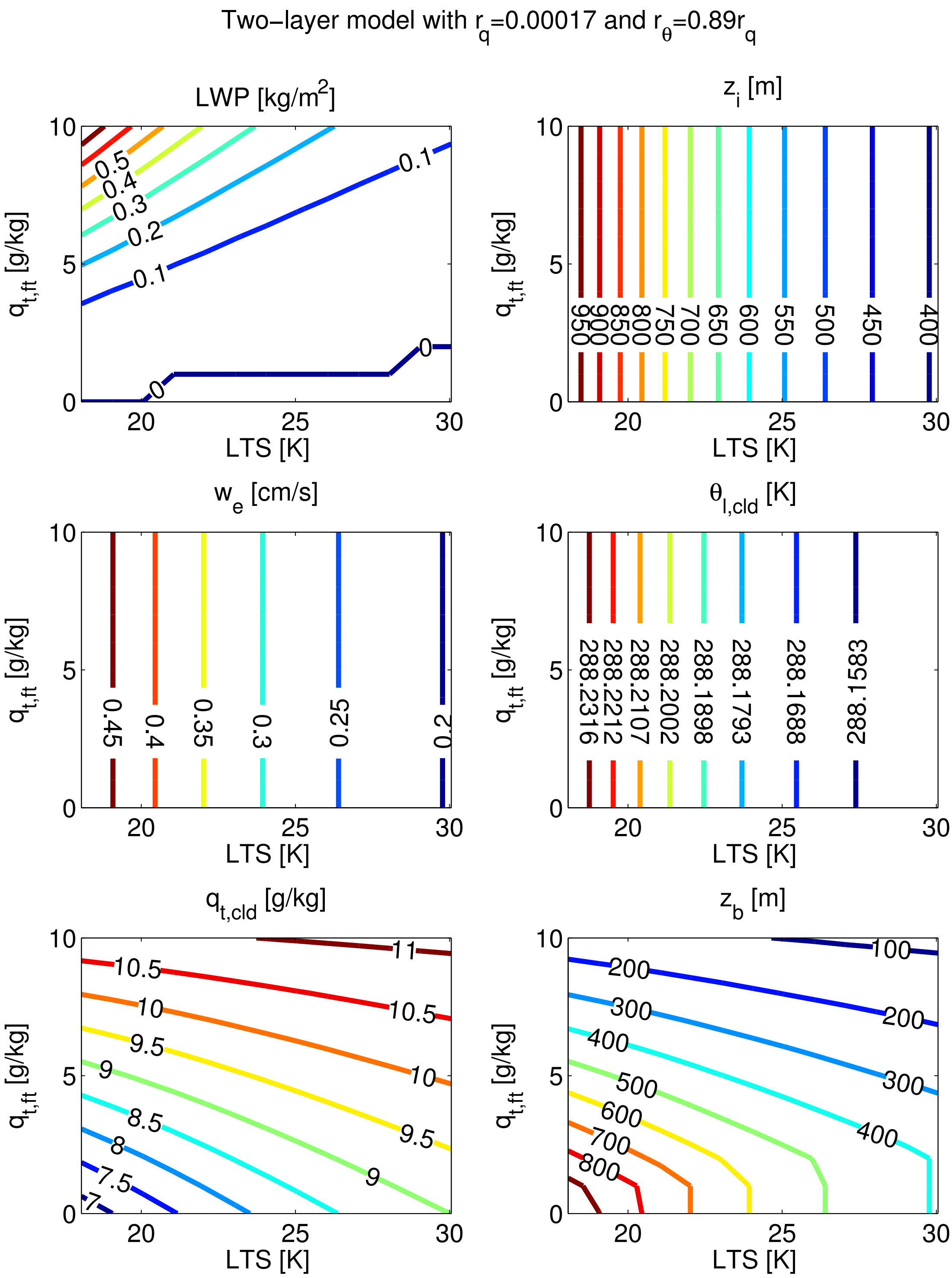

Figure 8.5 – Steady-state solutions of the two-layer model with $r_q = 1.7 \cdot 10^{-4}$ and $r_\theta = 0.89 r_q$.

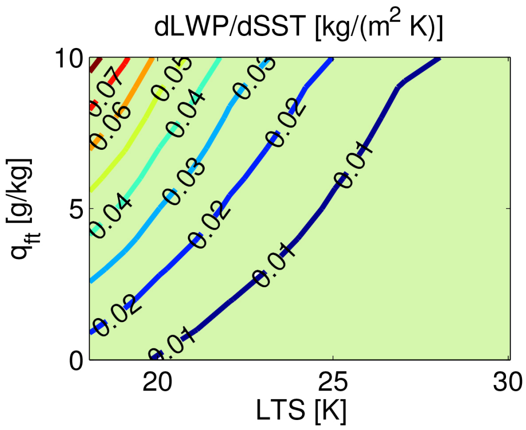

Figure 8.6 – Total response of the LWP in the single-layer model due to change in the SST. All responses of the LWP are positive.

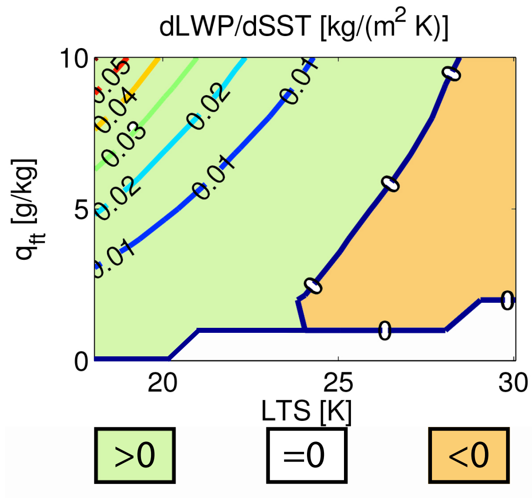

Figure 8.7 – Total response of the LWP in the two-layer model due to change in the SST. The decoupling parameters are $r_q = 1.7 \cdot 10^{-4}$ and $r_\theta = 0.89 r_q$.

a larger domain of free tropospheric conditions where there are no clouds at all, mostly for small $q_{\mathrm{t,ft}}$.
More decoupling ($1 \cdot 10^{-4} \leq r_q \leq 4 \cdot 10^{-4}$) results in a larger free-tropospheric domain where the response of the LWP is negative. The only positive response found here is for a combination of low LTS and high $q_{\mathrm{t,ft}}$.
Even more decoupling ($r_q \geq 5 \cdot 10^{-4}$) results in large free-tropospheric domains without clouds. For high $q_{\mathrm{t,ft}}$ there are still clouds predicted. The response of the LWP is in this case negative.
Overall, the decoupled system predicts no clouds for small $q_{\mathrm{t,ft}}$. For the other free tropospheric conditions the cloud response becomes smaller for higher decoupling rates resulting in an increasing area in the free-tropospheric phase-space where chloud thinning occurs instead of cloud thickening. Cloud thickening is only predicted for small decoupling parameters, low LTS and high $q_{\mathrm{t,ft}}$ but this thickening is less than predicted with the MLM.

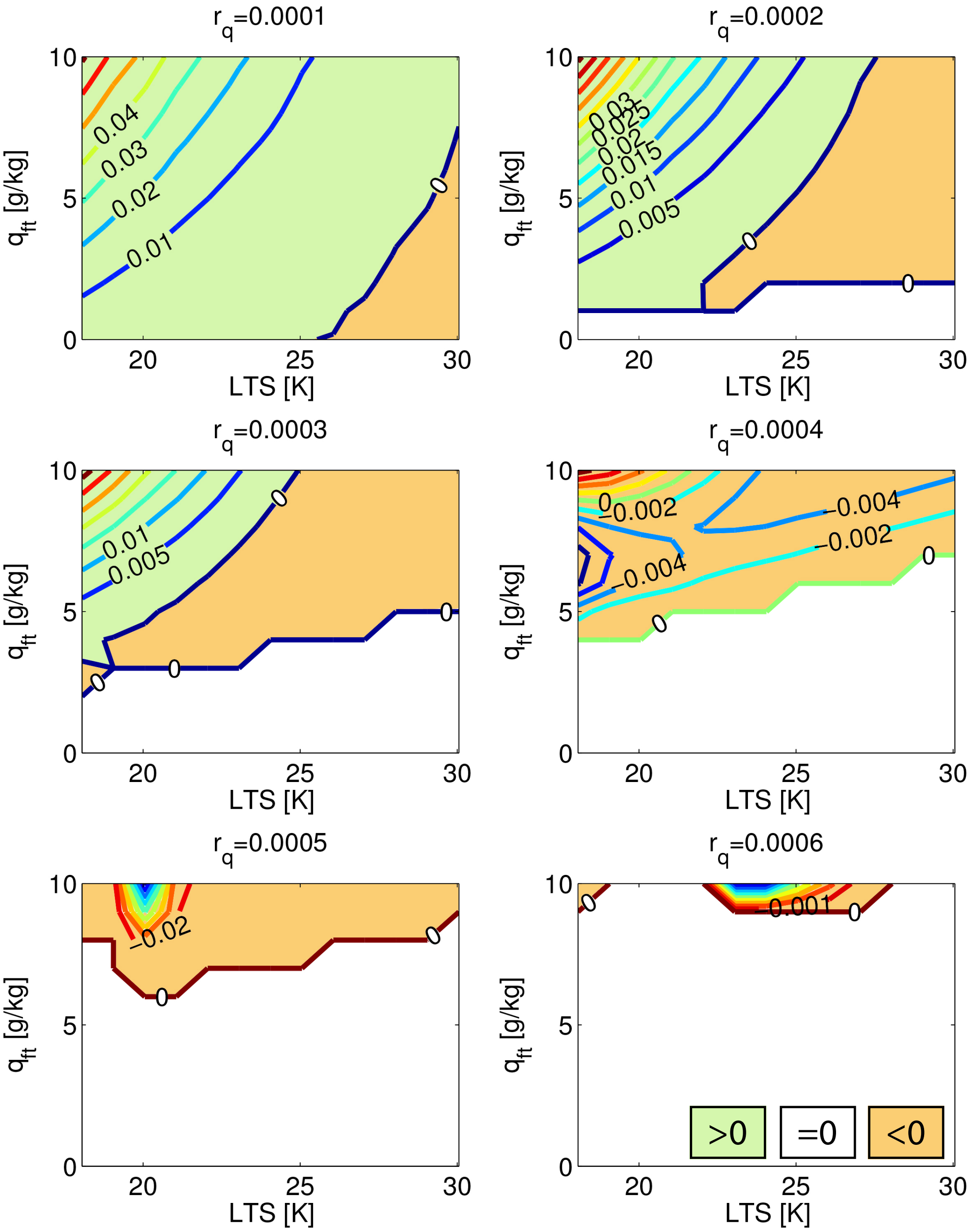

Figure 8.8 – Response of LWP to perturbed SST for different decoupling parameters with $r_\theta = 0.89 r_q$.

9 Conclusions

9.1 Transient solutions

A two-layer model that is more accurate than the MLM and able to predict the boundary layer evolution including the stratocumulus to cumulus transition is successfully developed in this research.
The two-layer model is able to predict a similar behaviour for the evolution of the boundary layer as the LES model for the ASTEX. Especially for the LWP, the results of the two-layer model are much more realistic than the results from the MLM. Moreover, the two-layer model can predict the cumulus cloud base similar to the results of the LES model, due to the condensation criterion $\mathrm{RH}_{\mathrm{crit}}$that is set in the sub-cloud layer.
The two-layer model developed in this research is able to predict the stratocumulus and stratocumulus to cumulus transition in a much better way than the MLM. The computational power needed for this model is small. The two-layer model is therefore a good tool to examine the effect of different perturbations in different cloud controlling factors.

The sensitivity of the development of the boundary layer to a different subsidence has been done by prescribing different divergences.
A smaller divergence led to a deeper BL and a larger LWP. In all two-layer model results for different divergences the LWP still decreases over time, indicating a cloud break-up. This was also found in the LES results from ASTEX.
Even though the entrainment rate is larger for a smaller subsidence, it results in a slower break-up of the stratocumulus cloud deck. The extra warming and drying of the cloud layer results in a higher cloud base, but it also results in a higher z_{i}. The increase in z_{i} is larger than the increase in z_{cb} due to a smaller subsidence rate, leading to a slower break-up. This confirms the earlier results from de Roode and van der Dussen [2010], Sandu and Stevens [2011], van der Dussen [2012], Bretherton et al. [2013].

9.2 Steady-state solutions

A strong dependency of the response of the LWP on the free tropospheric conditions was detected in the steady state solutions. This is in correspondance with the results fromde Roode et al. [2012]. The MLM predicted a cloud thickening and therefore a negative cloud radiative feedback for all free tropospheric conditions. A larger thickening was found for smaller LTS and higher $q_{\mathrm{t,ft}}$.
The two-layer model predicts cloud thickening or thinning depending on the free

tropospheric conditions and decoupling rates. For small $q_{\mathrm{t,ft}}$ the two-layer model does not predict stratocumulus at all. The two-layer model predicts a thickening for high $q_{\mathrm{t,ft}}$ and low LTS. This thickening is smaller than in the prediction of the MLM. For high LTS, the two-layer model predicts a cloud thinning. A larger decoupling rate results in a larger area where no stratocumulus clouds are predicted, a larger area where cloud thinning is predicted, and a smaller area where cloud thickening is predicted.
The two-layer model mostly predicts a cloud thinning for larger decoupling rates, resulting a positive cloud radiative feedback. This is in accordance with LES results of the cloud radiative feedback for a stratocumulus and a decoupled stratocumulus case.

10 Recommendations

The two-layer model developed in this research is able to predict the stratocumulus and stratocumulus to cumulus transition in a much better way than the MLM. The results of the two-layer model and the LES model give remarkably similar results for the ASTEX case. Some effects are not taken into account however.

The radiative cooling in the two-layer model is taken to be the average net radiation from ASTEX. As an improvement in the transient predictions of the two-layer model, the diurnal variation in the radiation could be implemented in the model.

Another process not taken into account is precipitation. As mentioned before, this means that the results are particularly applicable to a polluted environment in which clouds have a high droplet concentration and small drizzle fluxes. An MLM study of the effect of droplet concentration on the cloud thickness was done by Wood [2007].
For the ASTEX case however, van der Dussen found that the precipitation contribution is only significant in the first part of the transition.

To close the transient solutions of the two-layer model, a linear flux profile between the surface and the stratocumulus cloud base height was assumed. As explained in section 5.2, a linear flux profile between the sub-cloud layer height and the inversion layer height would also have been an option. Due to the decoupling, the cloud layer warms faster than the sub-cloud layer. The transient layer might therefore be warming with a tendency closer to the cloud layer than the sub-cloud layer and a linear flux profile between the sub-cloud layer height and the inversion layer height would perhaps be more realistic.

The radiative cooling in this research is taken constant. Dal Gesso et al. use a more realistic ΔF that is linearly dependent on q_t^+ in their steady-state experiments, based on earlier sensitivity studies of Fouquart [1988] and Morcrette [1991]. As one of the ranges in the phase-space considers $q_{\mathrm{t,ft}}$, the effect of a linearly dependent ΔF instead of a constant ΔF could easily be seen.

11 Acknowledgements

In the last year I learned a lot about clouds and about doing research. I would like to thank Stephan de Roode for his guidance and knowledge, but mostly for his enthusiasm which was really motivating.

Thanks to Sara Dal Gesso, for explaning more about the mixed layer model in a clear way. Also thanks to Johan van der Dussen, who shared his knowledge about ASTEX and made some valuable suggestions to improve my work.

I want to thank all the people from the Atmospheric Physics group, for the nice coffee and lunchbreaks, for making good use of every opportunity to bring cake and for trying to get me to run.

Thanks to my dear sisters and 'partners in physics', Marian and Margriet, for supporting me throughout my entire Applied Physics program.

Edwin, thank you for listening to my research stories and for always asking questions.

References

B.A. Albrecht. Marine boundary layer structure and fractional cloudiness. *Journal of Geophysical Research*, 100:14209–14222, 1995.

A.K. Betts. Relation between mean boundary-layer structure and cloudiness at the r/v valdivia during astex. *Journal of the Atmospheric Sciences*, 52:2752–2762, 1995.

C.S. Bretherton and R. Pincus. Cloudiness and marine boundary layer dynamics in the astex lagrangian experiments. part 1: Synoptic setting and vertical structure. *Journal of the atmospheric sciences*, 52(16):2707–2723, August 1995.

C.S. Bretherton and M.C. Wyant. Moisture transport, lower-tropospheric stability and decoupling of cloud-topped boundary layers. *Journal of the Atmospheric Sciences*, 54:148–167, 1997.

C.S. Bretherton, P.N. Blossey, and C.R. Jones. Mechanisms of marine low cloud sensitivity to idealized climate pperturbation: A single-les exploration extending the cgils cases. *Journal of advances in modeling earth systems*, 5:316–337, 2013.

P.M. Caldwell, Y. Zhang, and S.A. Klein. Cmip3 subtropical stratocumulus cloud feedback interpreted through a mixed-layer model. *Journal of Climate*, 2012. URL `http://climatemodeling.science.energy.gov/sites/default/files/publications/Caldwell_et12JClim-early.pdf`. Early online release.

J.W.M. Cuijpers. *Large-eddy simulation of cumulus convection*. PhD thesis, Technische Universiteit Delft, January 1994.

S. Dal Gesso, A.P. Siebesma, and S.R. de Roode. Evaluation of low-cloud climate feedback through single-column model equilibria. *Quart. J. Roy. Meteor. Soc.*, 2014a.

S. Dal Gesso, A.P. Siebesma, S.R. de Roode, and J.M. van Wessem. A mixed-layer model perspective on stratocumulus steady-states in a perturbed climate. *Quart. J. Roy. Meteor. Soc.*, February 2014b.

S.R. de Roode and J.J. van der Dussen. Large-eddy simulation of a stratocumulus to cumulus cloud transition as observed during astex. *Proceedings of the 19th symposium on boundary layers and turbulence*, August 2010. URL `http://www.srderoode.nl/PPT/Roode_ASTEX_Lag_Keystone.pdf`.

S.R. de Roode, P.G. Duynkerke, and H.J.J. Jonker. Large-eddy simulation: How large is large enough? *Journal of atmospheric science*, 61:403–421, 2004.

S.R. de Roode, A.P. Siebesma, S. Dal Gesso, H.J.J. Jonker, J. Schalkwijk, and Sival J. The stratocumulus response to a single perturbation in cloud controlling factors. *Journal of Climate*, 2012.

J.W. Deardorff. Usefulness of liquid-water potential temperature in a shallow-cloud model. *Journal of Applied Meteorology*, 15:98–102, 1975.

P.G. Duynkerke, P.J. Jonker, A. Chlond, M.C. van Zanten, J. Cuxart, P. Clark, E. Sanchez, G. Martin, G. Lenderink, and J. Teixeira. Intercomparison of three- and one-dimensional model ssimulation and aircraft observations of stratocumulus. *Boundary-Layer Meteorology*, 92:453–487, September 1999.

Y. Fouquart. Radiative transfer in climate models. In M.E. Schlesinger, editor, *Physically-Based Modelling and Simulation of Climate and Climatic Change*, volume 243 of *NATO ASI Series*, pages 223–283. Springer Netherlands, 1988. ISBN 978-94-010-7867-2. 10.1007/978-94-009-3041-4_5. URL `http://dx.doi.org/10.1007/978-94-009-3041-4_5`.

J.R. Garrat. *The atmospheric boundary layer.* Press Syndicate of the University of Cambridge, 1994.

D. K. Lilly. Models of cloud-topped mixed layers under a strong inversion. *Quart. J. Roy. Meteor. Soc.*, 94:292–309, 1968.

Met Office UK, 2014. URL `http://www.metoffice.gov.uk/learning/clouds/low-level-clouds`.

Jean-Jacques Morcrette. Radiation and cloud radiative properties in the european centre for medium range weather forecasts forecasting system. *Journal of Geophysical Research: Atmospheres*, 96(D5):9121–9132, 1991. ISSN 2156-2202. 10.1029/89JD01597. URL `http://dx.doi.org/10.1029/89JD01597`.

F.W. Murray. On the computation of saturation vapor pressure. *Journal of Applied Meteorology*, pages 203–204, August 1967.

S. Nicholls. The dynamics of stratocumulus: aircraft observations and comparisons with a mixed layer model. *Quart. J. Roy. Meteor. Soc.*, 110:783–820, 1984.

S. Nicholls and J. Leighton. An observational study of the structure of stratiform cloud sheets: Part 1: Structure. *Quart. J. Roy. Meteor. Soc.*, 112:431–460, 1985.

S. Park, C.B. Leovy, and M.A. Rozendaal. A new heuristic lagrangian marine boundary layer cloud model. *Journal of the atmospheric sciences*, 61:3002–3024, June 2004.

D.A. Randall, J.A. Coakley Jr., C.W. Fairall, R.A. Kropfli, and D.H. Lenschow. Outlook for research on subtropical marine stratiform clouds. *Bulletin of the American Meteorological Society*, 65:1290–1301, 1984.

D.P. Rogers and D. Koracin. Radiative transfer and turbulence in the cloud-topped marine atmospheric boundary layer. *Journal of the atmospheric sciences*, pages 1473–1486, 1992.

Jenny Ryan. The Meteo Times, September 2012. URL `http://www.meteotimes.net/2012/09/stratocumulus-clouds-dollymount-strand.html`.

I. Sandu and B. Stevens. On the factors modulating the stratocumulus to cumulus transitions. *Journal of atmospheric science*, 68:1865–1881, 2011.

M. Sidran. Broadband reflectance and emissivity of specular and rough water surfaces. *Applied Optics*, 20:3176–3183, 1981.

B. Stevens. Entrainment in stratocumulus-topped mixed layers. *Quart. J. Roy. Meteor. Soc.*, 2003.

R.B. Stull. *An Introduction to Boundary Layer Meteorology*. Kluwer Academic Publishers, 1988.

J.D. Turton and S. Nicholls. A study of the diurnal variation of stratocumulus using a multiple mixed layer model. *Quart. J. Roy. Meteor. Soc.*, 1987.

J.J. van der Dussen. Large eddy simulation sensitivity experiments of the astex stratocumulus to cumulus transition. *Proceedings of the 20th Symposium on boundary layers and turbulence*, 2012. URL `https://ams.confex.com/ams/20BLT18AirSea/webprogram/Paper208717.html`.

J.J. van der Dussen, S.R. de Roode, A.S. Ackerman, P.N. Blossey, C.S. Bretherton, M.J. Kurowski, A.P. Lock, R.A.J. Neggers, I. Sandu, and A.P. Siebesma. The gass/euclipse model for intercomparison of the stratocumulus transition as observed during astex: Les results. *Journal of advances in modeling earth systems*, 5:483–499, 2013.

M.C. van Zanten. *Entrainment processes in stratocumulus*. PhD thesis, Universiteit Utrecht, 2000.

S.G. Warren, C.J. Hahn, J. London, R.M. Chervin, and R.L. Jenne. Global distribution of total cloud cover and cloud type amounts over the ocean. *NCAR Technical note TN-317+STR*, 1988.

K.D. Williams and M.J. Webb. A quantitative performance assessment of cloud regimes in climate models. *Climate Dynamics*, 33:141–157, 2009.

R. Wood. Cancellation of aerosol indirect effect in marine stratocumulus through cloud thinning. *Journal of the atmospheric sciences*, 64:2657–2669, 2007.

R. Wood. Stratocumulus clouds. *Monthly wheather review*, 140:2373–2423, 2012.

R. Wood and C.S. Bretherton. Boundary layer depth, entrainment and decoupling in the cloud-capped subtropical and tropical marine boundary layer. *Journal of Climate*, 17:3576–3588, 2004.

M.C. Wyant and C.S. Bretherton. Numerical simulation and a conceptual model of the stratocumulus to trade cumulus transition. *Journal of the atmospheric sciences*, 54:168–192, 1997.

M. Zhang, C.S. Bretherton, P.N. Blossey, P.H. Austin, Bacmeister J.T., S. Bony, F. Brient, S.K. cheedela, A. Cheng, A.D. Del Genio, S.R. de Roode, S. Endo, C.N. Franklin, J. Golaz, C. Hannay, T. Heus, F.A. Isotta, J. Dufresne, I. Kang, H. Kawai, M. Köhler, V.E. Larson, Y. Liu, A.P. Lock, U. Lohmann, M.F. Khairoutdinov, A.M. Molod, R.A.J. Neggers, P. Rasch, I. Sandu, R. Senkbeil, A.P. Siebesma, C. Siegenthaler-Le Drian, B. Stevens, M.J. Suarez, K. Xu, K. von Salzen, M.J. Webb, A. Wolf, and M. Zhao. Cgils: Results from the first phase of an international project to understand the physical mechanisms of low cloud feedbacks in single column models. *Journal of advances in modeling earth systems*, 5:826–842, 2013.

Y. Zhang. Low-cloud fraction, lower-tropospheric stability and large-scale divergence. *Journal of Climate*, 22:48274844, 2009.

A List of Symbols

Abbreviation	**Meaning**
A	Scaling factor
$A_{d,w}$	Dry and wet coefficient
$B_{d,w}$	Dry and wet coefficient
C_d	Drag coefficient
D	Divergence of wind velocity
F_ψ	Flux of conserved variable ψ
L_v	Specific latent heat
LES	Large eddy simulation
LTS	Lower tropospheric stability
LWP	Liquid water path
MLM	Mixed layer model
R	Ideal gas constant
Ri	Richardson number
S_ψ	Source term for conserved variable ψ
SST	Sea surface temperature
T	Temperature
U	Horizontal wind velocity
c_p	Specific heat capacity
e_s	Saturation vapor pressure
f_ψ	Flux ratio
g	Gravity constant
m	Mass
p	Pressure
p_0	Reference pressure
q_l	Liquid specific humidity
q_{sat}	Saturation specific humidity
q_t	Total specific humidity
r_k	Mixing ratio
r_ψ	Decoupling parameter for conserved variable ψ
s_l	Liquid static energy
w	Velocity in vertical direction
$\overline{w}$	Large-scale subsidence velocity
w_{e}	Entrainment rate
z_{cb}	Cloud base height
z_{cld}	Cloud thickness
z_{i}	Height of inversion layer
z_{ML}	Height of sub-cloud layer

Abbreviation	**Meaning**
Γ_ψ	Lapse rate in free troposphere
Θ	Virtual potential temperature flux
Π	Exner function
α_ψ	Decoupling parameter for conserved variable ψ
ϵ	Emmissivity
η	Efficiency factor in entrainment parameterisation
θ	Potential temperature
θ_l	Liquid potential temperature
θ_v	Virtual potential temperature
ϕ	Cloud controlling factor
ψ	Thermodynamic property, q_t or θ_l
ψ^+	ψ just above the inversion
ρ	Density
σ	Stefan-Boltzmann constant

B Derivations of equations

B.1 Potential Temperature

An air parcel at different heights will experience different pressures and also different temperatures. To be able to compare air parcels, the potential temperature has been introduced. This potential temperature is a temperature that is not influenced if a parcel of air moves adiabatically. The equation for potential temperature can be deduced from the first law of thermodynamics;

$$du = dq - dw = dq - pdv. \tag{B.1}$$

With the use of the equation for the enthalpy

$$dh = du + pdv + vdp, \tag{B.2}$$

and using the definition for the isobaric specific heat

$$c_p \equiv \left(\frac{\partial h}{\partial T}\right)_p, \tag{B.3}$$

the first law can be rewritten as

$$dq = c_p dT - vdp. \tag{B.4}$$

When considering an air parcel that undergoes an adiabatic process, no heat exchange occurs, $dq = 0$. Using the ideal gas law, equation B.4 becomes

$$\frac{c_p}{T} dT = \frac{R_\mathrm{d}}{p} dp, \tag{B.5}$$

which can be integrated from a pressure p and temperature T to a reference pressure p_0 and reference temperature θ:

$$\int_T^\theta \frac{c_p}{T} dT = \int_p^{p_0} \frac{R_\mathrm{d}}{p} dp. \tag{B.6}$$

From this the potential temperature θ can be found:

$$\theta = T \left(\frac{p_0}{p}\right)^{\frac{R_\mathrm{d}}{c_p}}. \tag{B.7}$$

Here the potential temperature and the actual temperature are related by the so called exner function Π

$$\Pi = \left(\frac{p}{p_0}\right)^{\frac{R_\mathrm{d}}{c_p}} = \frac{T}{\theta}. \tag{B.8}$$

B.2 Mixed Layer Model budget equation

For any conserved variable ψ the conservation equation in differential form can be written as

$$\frac{D\psi}{Dt} = \frac{\partial \psi}{\partial t} + u_i \frac{\partial \psi}{\partial x_i} = \frac{\partial S}{\partial x_i}, \tag{B.9}$$

where S represents a flux source. Using the Reynolds averaging method and assuming small mean horizontal gradients, it can be derived that

$$\frac{\partial \overline{\psi}}{\partial t} = -\overline{w}\frac{\partial \overline{\psi}}{\partial t} - \frac{\partial \overline{w'\psi'}}{\partial z} - \frac{\partial \overline{S}}{\partial z}. \tag{B.10}$$

In the boundary layer $\overline{\psi} = \psi_{ML}$ is constant with height up to the base of the inversion layer. Vertical integration of equation (B.10) then gives

$$z_i \frac{\partial \psi_{ML}}{\partial t} = -\overline{w'\psi'}|_{z_i} + \overline{w'\psi'}|_0 - \overline{S_\psi}|_{z_i} + \overline{S_\psi}|_0, \tag{B.11}$$

where the subscript z_i refers to the values at the top of the mixed layer and the subscript 0 refers to the surface values. The conserved variables ψ are governed by the surface flux $F_{\psi,0} = \overline{w'\psi'}|_0$, the flux at the top of the inversion layer $F_{\psi,T} = \overline{w'\psi'}|_{z_i}$ and the total change between the source term at the surface and at the top of the boundary layer $\Delta S_\psi = \overline{S_\psi}|_0 - \overline{S_\psi}|_{z_i}$. Equation (B.11) can then be rewritten as

$$z_i \frac{\partial \psi_{ML}}{\partial t} = F_{\psi,0} - F_{\psi,T} - \Delta S_\psi. \tag{B.12}$$

The surface flux $\overline{w'\psi'}|_0$ can be obtained by

$$\overline{w'\psi'}|_0 = C_d U(\psi_0 - \psi_{ML}), \tag{B.13}$$

with drag coefficient C_d and U the horizontal wind speed. The flux at the top of the inversion layer is taken as

$$\overline{w'\psi'}|_{z_i} = -w_e(\psi(z_i^+) - \psi_{ML}), \tag{B.14}$$

with entrainment w_e and the jump of conserved variable ψ across the inversion [Lilly, 1968]. The values at z_i^+ are just above the inversion layer, which is considered to have a very small thickness. The conservation equation can then be rewritten as

$$z_i \frac{\partial \psi_{ML}}{\partial t} = C_d U(\psi_0 - \psi_{ML}) + w_e(\psi(z_i^+) - \psi_{ML}) - \Delta S_\psi. \tag{B.15}$$